HHS Public Access

Author manuscript

Cell Rep. Author manuscript; available in PMC 2023 April 18.

Published in final edited form as:

Cell Rep. 2023 March 28; 42(3): 112273. doi:10.1016/j.celrep.2023.112273.

Alternative splicing of *HDAC7* regulates its interaction with 14-3-3 proteins to alter histone marks and target gene expression

Laura M. Agosto[1,2], **Michael J. Mallory**[1], **Max B. Ferretti**[1,3], **Davia Blake**[1,4], **Keegan S. Krick**[1,5], **Matthew R. Gazzara**[1,6], **Benjamin A. Garcia**[1,7,8], **Kristen W. Lynch**[1,2,4,5,9,*]

[1]Department of Biochemistry and Biophysics, University of Pennsylvania, Philadelphia, PA 19104, USA

[2]Biochemistry and Molecular Biophysics Graduate Group, University of Pennsylvania, Philadelphia, PA 19104, USA

[3]Department of Pathology, University of Pennsylvania, Philadelphia, PA 19104, USA

[4]Immunology Graduate Group, University of Pennsylvania, Philadelphia, PA 19104, USA

[5]Cell and Molecular Biology Graduate Group, University of Pennsylvania, Philadelphia, PA 19104, USA

[6]Genomic and Computational Biology Graduate Group, University of Pennsylvania, Philadelphia, PA 19104, USA

[7]Epigenetics Institute, Perelman School of Medicine, University of Pennsylvania, Philadelphia, PA 19104, USA

[8]Present address: Department of Biochemistry and Molecular Biophysics, Washington University School of Medicine, St. Louis, MO 63110, USA

[9]Lead contact

SUMMARY

Chromatin regulation and alternative splicing are both critical mechanisms guiding gene expression. Studies have demonstrated that histone modifications can influence alternative splicing decisions, but less is known about how alternative splicing may impact chromatin. Here, we demonstrate that several genes encoding histone-modifying enzymes are alternatively spliced downstream of T cell signaling pathways, including *HDAC7*, a gene previously implicated in controlling gene expression and differentiation in T cells. Using CRISPR-Cas9 gene editing

*Correspondence: klync@pennmedicine.upenn.edu.

AUTHOR CONTRIBUTIONS

L.M.A., M.J.M., M.B.F., D.B., K.S.K., and M.R.G. conducted the experiments and analyzed data, and L.M.A., B.A.G., and K.W.L. designed experiments, directed the project, and wrote the paper.

SUPPLEMENTAL INFORMATION

Supplemental information can be found online at https://doi.org/10.1016/j.celrep.2023.112273.

DECLARATION OF INTERESTS

The authors declare no competing interests.

and cDNA expression, we show that differential inclusion of HDAC7 exon 9 controls the interaction of HDAC7 with protein chaperones, resulting in changes to histone modifications and gene expression. Notably, the long isoform, which is induced by the RNA-binding protein CELF2, promotes expression of several critical T cell surface proteins including CD3, CD28, and CD69. Thus, we demonstrate that alternative splicing of *HDAC7* has a global impact on histone modification and gene expression that contributes to T cell development.

In brief

Chromatin regulation and alternative splicing are independent mechanisms increasingly recognized to experience cross-talk to tune gene expression. Agosto et al. show that alternative splicing of the histone deacetylase HDAC7 in T cells controls its interaction with protein chaperones, resulting in changes to histone modifications and expression of key activation markers.

Graphical Abstract

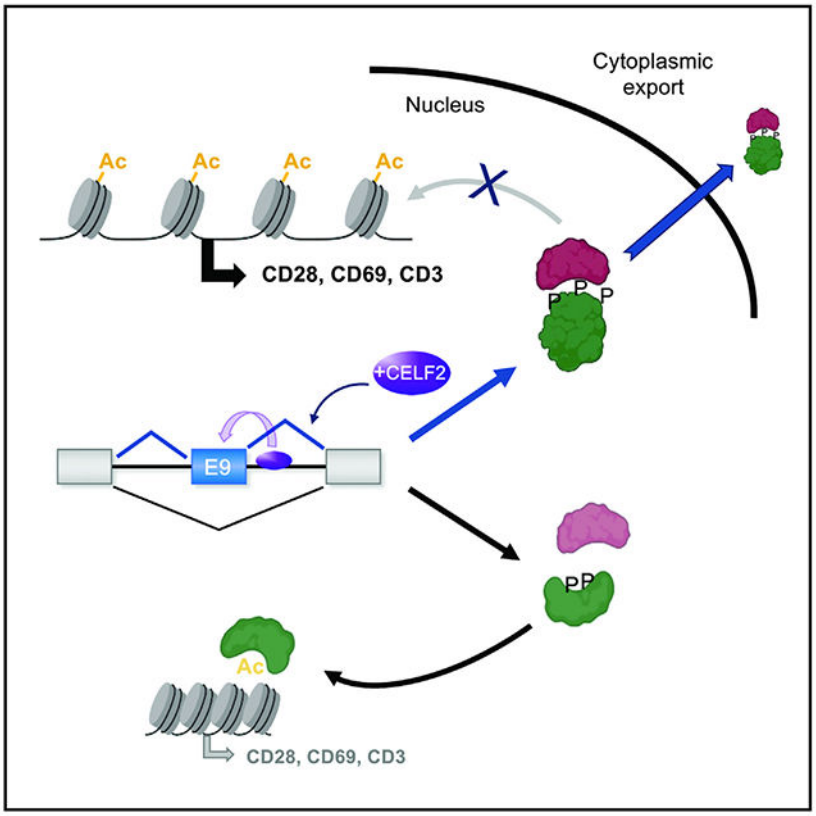

INTRODUCTION

Gene expression is regulated by many mechanisms that together determine how much protein is made from a particular gene. Examples of such mechanisms include chromatin accessibility, transcription elongation rates, pre-mRNA alternative splicing, mRNA degradation, translation efficiency, and protein degradation. Interestingly, any one

of these mechanisms can be regulated by itself (generating a feedback loop) and/or by another mechanism, as well as through cell signaling events and post-transcriptional or post-translational modifications (PTMs). Thus, the interplay between the aforementioned mechanisms can be viewed as layers of a network of "coordinated steps in gene expression to control specific cellular activities."[1]

Two steps of gene expression for which there has been particular evidence of cross-talk or coordination are chromatin modification (referred to here as epigenetics) and alternative splicing.[2,3] For example, some histone PTMs, such as histone H3 lysine 36 trimethylation (H3K36me3), are preferentially found at exonic vs. intronic regions.[4–7] The current understanding in the field for cross-talk between chromatin, transcription, and splicing can be summarized in three non-exclusive models: a kinetic model for RNA polyermase II (RNA Pol II) pausing that creates a "window of opportunity" for splice sites to be recognized co-transcriptionally,[8] and two inverse models in which RNA Pol II and/or specific histone PTMs promote inclusion of variable pre-mRNA sequences, or conversely, splicing factors direct the deposition of histone PTMs on actively transcribed genes.[2,3,9] However, the extent to which alternative splicing might control epigenetics in *trans* to affect programs of transcription events has been less well explored.

Here, we investigate this reciprocal interplay of splicing and epigenetics, namely how alternative splicing of histone-modifying enzymes (HMEs) can impact their activity to alter the epigenetic and gene expression landscape. Some evidence for the regulation of HMEs by alternative splicing has already been shown in the case of the methytransferase encoding gene *EHMT2* (aka G9a and KMT1C). Specifically, inclusion of exon 10 results in an EHMT2 isoform that preferentially localizes to the nucleus, thus increasing histone H3 lysine 9 dimethylation (H3K9me2) levels, and promotes neuronal differentiation.[10,11] Interestingly, genes encoding several other HMEs have been described to exhibit multiple isoforms, including the gene encoding HDAC7. However, the functional impact of alternative splicing of these additional HMEs on epigenetics and gene expression has not been explored.

HDAC7 is a ~103 kDa protein that belongs to the class IIa family of histone deacetylases (HDACs; also including HDACs 4/5/9) that remove acetyl groups from substrate lysine residues, thus acting as PTM "erasers."[12,13] Since their discovery 20 years ago, several groups have studied class IIa HDACs and uncovered three features that distinguish them from other HDAC families. First, the polypeptide sequence is divided into two main segments, N-terminal and C-terminal. The N-terminal segment is a regulatory domain that mediates interactions with transcription factors and other proteins, while the C-terminal (C-term) segment contains the deacetylase domain and binding sites for co-repressors, such as SMRT/NCoR and SIN3A.[14–19] The second distinguishing feature of the class IIa family is their nucleocytoplasmic shuttling mediated by signal-induced phosphorylation at conserved serine residues in the regulatory N-term segment and binding of phosphorylated (phospho)-serine by 14-3-3 proteins.[19] Lastly, class IIa HDACs are expressed in a tissue-specific manner. Notably, *HDAC7* transcript expression is highest in the heart, lungs, skeletal muscle, and thymus,[20] and genetic manipulation experiments have shown that HDAC7 protein is necessary to maintain proper identity and development of lymphocytes

including thymocytes.[20–27] Specifically, phosphorylation of HDAC7 by signaling cascades downstream of the T cell receptor (TCR) increase its interaction with 14-3-3 proteins and sequestration from the nucleus to remove HDAC7-mediated repression of key activation genes.[28] Moreover, in thymocytes, genes that are induced upon knockout of HDAC7 overlap significantly with those that are upregulated upon positive selection of CD4/CD8-double-positive (DP) cells, suggesting that downregulation of HDAC7 activity is a driver of gene expression in response to pre-TCR signaling in DP thymocytes.[27]

Here, we show that several HME genes exhibit shifts in alternative splicing upon induction of T cell signaling, including a dramatic increase in inclusion of exon 9 of the gene encoding HDAC7. Using CRISPR-engineered monoclonal cell lines that constitutively include or skip *HDAC7-E9*, we found that inclusion of *E9* results in higher protein expression and stability upon T cell stimulation, as well as altered histone PTMs and gene expression including increased expression of TCRs in both unstimulated and stimulated cell conditions. Moreover, we find that the longer isoform of HDAC7, encoded by exon 9-included mRNA, has increased interaction with 14-3-3 proteins compared with the shorter HDAC7 isoform. Since 14-3-3 proteins are known to stabilize and relocalize HDAC7 to the cytoplasm, the change in interaction with 14-3-3 proteins is consistent with the functional impact of *HDAC7* alternative splicing on the transcription landscape. Finally, we show that *HDAC7-E9* inclusion is controlled by the RNA-binding protein CELF2 and increases during thymic development in a manner that correlates with increased expression of both CELF2 and known HDAC7-regulated target genes.[27] In sum, our data demonstrate that *HDAC7* alternative splicing contributes to gene activation in response to pre-TCR signaling, as occurs during thymic development. Our work also provides further evidence for a role of HDAC7 in T cell biology and highlights an additional model for how the interplay between splicing and epigenetics can be achieved.

RESULTS

Identification of alternatively spliced HME genes upon T cell stimulation

We previously utilized the MAJIQ algorithm to analyze RNA sequencing (RNA-seq) data and confidently identify changes in splicing patterns between unstimulated and PMA-stimulated Jurkat T cells (Figure 1A),[29–31] which serves as a model for pre-TCR signaling in developing thymocytes.[32] In total, we identified 2,010 local splice variations (LSVs), corresponding to 1,392 alternatively spliced genes (ASGs), that significantly change after 48 h of PMA stimulation (change in percent spliced in (ΔPSI) $\geq |20\%|$, $p \geq 0.95$; Figure 1B).[30] Gene Ontology (GO) enrichment analysis of the genes that undergo splicing changes revealed that several of the most enriched biological processes correspond to gene regulatory activities such as RNA/mRNA splicing and processing (7/15 categories) and chromatin modification and organization (4/15 categories; Figure S1A).[33] Likewise, the top cellular components highlight several chromatin/chromosome organization categories (8/15 categories), as well as protein/histone acetyltransferase and deacetylase complexes (5/15 categories; Figure S1B). Lastly, the gene set's top molecular functions include several enzymatic categories relevant to gene regulation, such as methyltransferases and kinases, guanyl-nucleotide factors and regulators, and protein/RNA binding (Figure

S1C). The enrichment of RNA-binding proteins and splicing activities among the ASGs is consistent with previous work demonstrating auto- and cross-regulatory loops among splicing factors.[30,34] However, the enrichment of chromatin and histone regulators among the ASGs is less well documented and suggests that splicing regulation may also indirectly impact chromatin modification and gene expression by controlling the activity of epigenetic regulators.

To determine which of the 2,010 significant splicing changes could directly impact chromatin marks, we cross-referenced the 1,392 ASGs with an in-house-compiled list of chromatin regulators that includes writer and eraser enzymes, PTM reader proteins, and chromatin remodelers, among other non-catalytic complex subunits. Indeed, we found that 81 alternative splicing events, corresponding to 54 chromatin regulator genes, undergo stimulation-induced changes (Figure 1B). To directly study the effects of alternative splicing on chromatin, we focused on splicing changes occurring in transcripts encoding HMEs and found that 18 out of the 54 genes that exhibit stimulation-induced splicing regulation encode HME transcripts (Figure 1B). The HME genes that exhibit stimulation-responsive alternative splicing are *ATR, EHMT2, HDAC4, HDAC6, HDAC7, KAT2A, KAT6A, KDM1A, KDM4B, NSD2, PKN1, PRDM2, PRMT1*, *PRMT7, SETDB2, TAF1*, *USP21*, and *UTY*. We further confirmed several of these events by low-cycle RT-PCR (Figures 1C and S1D). Overall, the majority of the splicing events follow the cassette exon (CE) splicing pattern (regulated full-length exon), while a smaller fraction of events are categorized as intron retention (IR), alternative splice site, or alternative first exon (AFE/transcription start site [TSS]; Figure S1D). In sum, our analysis reveals that several chromatin-regulatory and/or HME genes are regulated by alternative splicing upon T cell stimulation.

We hypothesize that the change in splicing of genes encoding these HMEs may alter protein expression or function in a way that leads to changes in chromatin and histone PTMs and, ultimately, to alterations in gene expression. Indeed, it has already been shown that one of the stimulation-induced changes in splicing we observe, namely regulated inclusion of exon 10 of *EHMT2* (also known as [aka] G9a), modulates the subcellular localization of the encoded protein such that histone H3 methylation is reduced in cells that express more of this isoform.[10,11] Given this precedent, we were interested in determining the functional consequence of stimulation-induced splicing of *HDAC7*, the gene for which we observe the next largest change in inclusion of a CE in the coding sequence after *EHMT2* (Figure S1D).

Inclusion of *HDAC7-E9* leads to increased HDAC7 protein expression and stability

The stimulation-induced splicing change in *HDAC7* quantified by MAJIQ corresponds to a predicted 44% increase in inclusion of *HDAC7* exon 9 (*HDAC7-E9*) upon T cell stimulation (Figure S1D). We validated this splicing event using low-cycle RT-PCR and quantified the increase in exon inclusion as showing an average change in inclusion (ΔPSI) of 21% across multiple experiments (up to 40% in some individual replicates; Figures 1C, 2A, and 2B). Given the large change in inclusion of *HDAC7-E9*, we wanted to determine if the *HDAC7* mRNA and/or protein were also differentially expressed upon T cell stimulation. Using radiolabeled RT-PCR (Figure 2C) and qRT-PCR (Figure 2D), we quantified a 2.7-fold increase in total *HDAC7* transcript abundance after PMA stimulation. Analogously, we

observed a 5- to 10-fold increase in HDAC7 protein by western blot (Figure 2E) and nano-liquid chromatography coupled to tandem mass spectrometry (nano-LC-MS/MS) (Figure 2F).

In humans, the *HDAC7* gene has two alternative promoters, with the proximal promoter dominating in primary and cultured T cells based on RNA-seq read coverage. When *HDAC7-E9* is included, the resultant encoded protein is 952 amino acids and includes a nuclear localization signal (NLS); a characterized and a putative nuclear export signal (NES); a deacetylase domain; sites of co-repressor interaction; and multiple sites of known modifications (Figure S2). By contrast, skipping of the 111 nucleotide *HDAC7-E9* results in an in-frame deletion of 37 amino acids within the N-term adapter domain and a final protein size of 915 amino acids. Sequence analysis of the peptide encoded by *E9* predicts a putative CRM1 NES.[35] However, this is not the biochemically characterized/annotated HDAC7 NES.[18,36] Additionally, the *E9* peptide exists between two key serine phosphorylation sites (pSer181/358 for the longer isoform) that help mediate binding of 14-3-3 proteins and nuclear export of HDAC7.[19] Importantly, the phosphorylation-induced 14-3-3 binding to HDAC7 has also been implicated in higher HDAC7 protein stability.[37]

To determine if the observed increase in HDAC7 protein upon stimulation is driven by increased transcription and/or alternative inclusion of *E9*, we first analyzed mRNA and protein across several time points between 0 and 48 h of stimulation. Both qRT-PCR and low-cycle RT-PCR of the total *HDAC7* transcript demonstrated a ~2-fold increase in *HDAC7* transcript abundance by 12 h post-stimulation, which further increased to 3.2-fold by 48 h (Figure 2G). Interestingly, low-cycle RT-PCR further revealed a bimodal pattern of splicing regulation in which *E9* inclusion is dramatically reduced during the first 12 h of stimulation before steadily increasing to ~50% inclusion by 48 h (Figure 2H). Finally, by western blot, we find that the largest increase in detectable HDAC7 protein occurs between 12 and 24 h following stimulation (Figure 2I), coincident with the timing of *HDAC7-E9* inclusion.

Given the temporal correlation between the inclusion of *HDAC7-E9* and protein abundance, we next directly tested the effect of *HDAC7-E9* inclusion on HDAC7 protein expression by generating cell lines that exclusively express or exclusively skip *HDAC7-E9* using CRISPR-Cas9 gene editing (Figure 3A). Homozygous deletion of exon 9 and adjacent intronic regions resulted in cell lines that only express the exon 9-excluded version of HDAC7 (i.e., ΔE9), while fusion of exons 9 and 10 yielded cells that only express the exon 9-included version of HDAC7 (iE9). We validated the CRISPR clones by Sanger sequencing of both the genomic DNA (gDNA) and resultant mRNA transcripts products after PCR/RT-PCR amplification (Figures 3B and S3A–S3C). Next, we quantified the *HDAC7* mRNA (Figure 3C) and protein (Figure 3D) expression in the wild-type (WT) and CRISPR cell lines by qRT-PCR and western blot, respectively. Strikingly, under both unstimulated and stimulated conditions, iE9 cells expressed dramatically more protein than either the WT or ΔE9 cells (Figure 3D). While some of this increased protein might be attributable to higher levels of *HDAC7* mRNA in the iE9 cells, the difference in protein observed was greater than the difference in mRNA (Figures 3C vs. 3D). Of note, both CRISPR cell line extracts exhibit two distinctly migrating bands per sample (due perhaps to PTMs), while the signal in the

WT lane is more diffuse, indicating the presence of several bands consistent with the WT cells expressing a mix of iE9 and ΔE9 proteins (Figure 3D).

Given the previous demonstration that HDAC7 protein stability is enhanced by the phosphorylation-induced binding of 14-3-3 proteins,[37] we wondered whether a difference in stability between the HDAC7 isoforms could explain the difference in abundance between HDAC7iE9 and HDAC7ΔE9. To test this, we treated both stimulated and unstimulated cells with cycloheximide (CHX) to block translation and assessed protein abundance by western blot (Figures S3D and S3E). Consistent with other studies demonstrating that T cell signaling induces HDAC7 phosphorylation and 14-3-3 association,[28] we observe an increase in the half-life of both iE9 and ΔE9 isoforms in stimulated cells compared with unstimulated controls (Figure 3E, solid vs. dotted lines). Moreover, our results show that the stability of the iE9 isoform is at least double that of ΔE9 under these stimulated conditions (Figure 3E, solid lines), consistent with the marked increase in iE9 vs. ΔE9 proteins under steady-state conditions (Figure 3D).

While *HDAC7-E9* does not encode any of the phosphorylation sites that are necessary for binding by 14-3-3 proteins, it is within the region of HDAC7 with which 14-3-3 proteins interact. We therefore hypothesized that the greater stability of HDAC7iE9 compared with HDAC7ΔE9 results from the deletion of the *HDAC7-E9*-encoded peptide and a concomitant reduction in the interaction of 14-3-3 proteins with HDAC7. To investigate this possibility, we generated cells lines that expressed either HDAC7 isoform cDNA fused to an N-term FLAG tag. After 48 h of PMA stimulation, co-immunoprecipitation (coIP) of FLAG-HDAC7 isoforms showed that 14-3-3 proteins are more abundantly associated with HDAC7iE9 vs. HDAC7ΔE9, as quantified by either western blot or nano-LC/MS-MS (Figures 3F and 3G). By contrast, the HDAC7ΔE9 isoform associates more efficiently with LEF1 (Figure 3F), a transcription factor that has been implicated to interact with HDAC7.[38] Therefore, we conclude that inclusion of *HDAC7-E9* promotes association with 14-3-3 proteins, which leads to increased protein stability and steady-state protein expression.

Inclusion of *HDAC7-E9* correlates with increased histone acetylation and gene expression

In addition to increasing protein stability, the interaction of 14-3-3 proteins with HDAC7 has been shown to sequester HDAC7 from the nucleus. [19,28] Furthermore, reduction of HDAC7 from the nucleus by knockdown or 14-3-3 sequestration results in changes in histone PTMs and transcription.[21,22,28] Consistently, we find that the increased interaction of the iE9 isoform of HDAC7 with 14-3-3 proteins relative to the ΔE9 isoform correlates with a decrease in interaction with at least one transcription factor, LEF1 (Figure 3F), and histone H3 (Figure S4A). We thus sought to determine the impact of *HDAC7-E9* inclusion on histone PTMs and, ultimately, on gene expression. First, we compared histone PTMs (hPTMs) in the ΔE9 and iE9 CRISPR cell lines using a quantitative proteomics nano-LC-MS/MS analysis pipeline.[39,40] Notably, we observe multiple differences in hPTM abundance between the cells expressing exclusively HDAC7iE9 vs. HDAC7ΔE9, most significantly in the canonical and variant histone H3 proteins (Figures 4A and S4B). Specifically, iE9-expressing cells have higher global levels of H3 acetylation and some reduction in H3 methylation than cells expressing exclusively the ΔE9 isoform, especially in unstimulated

conditions (Figures 4A and S4B). We further validated some of the nano-LC-MS/MS acetylation results by immunoblotting intact histones obtained from WT, ΔE9, and iE9 cells with available PTM-specific antibodies (Figure 4B). Notably, differences in H3 acetylation are also observed when comparing iE9 cells against WT cells, consistent with WT cells expressing 50% or more of the ΔE9 isoform (Figure 4B).

Changes in acetylation of histones often result in altered transcription.[41–43] Thus, the observed differences in hPTMs between the iE9 and ΔE9 cells suggest that these cells may also exhibit differential gene expression. To test this prediction, we analyzed gene expression in our WT, ΔE9, and iE9 cell lines, under both unstimulated and stimulated conditions, by RNA-seq. The principal-component analysis (PCA) shows that components 1 and 2 (PC1 and PC2) explain 73% and 12% of the variability within the dataset, respectively (Figure 4C). As expected, PC1 variability reflects the differences in cell stimulation, while, strikingly, the driver of PC2 variance is the iE9 cell line, suggesting that these cells have a markedly different transcriptional program than WT and ΔE9 cells. Indeed, after applying filter cutoffs of $\log_2$ fold change $\geq|2|$, adjusted p value ≤ 0.05, and base mean ≥ 20, we find virtually no differences in the transcription profile between WT and ΔE9 cells (Figures 4D and S5), while there are 277 differentially expressed genes (DEGs) between iE9 and WT in unstimulated cells and 222 in stimulated conditions (in total, 409 DEGs combined; Figure 4D; Data S1). Similarly, we find 235 DEGs between iE9 and ΔE9 cells in unstimulated cells and 229 in stimulated conditions (Figure S5A). Interestingly, most of the changes we observe between iE9 and WT cells in unstimulated cells mimic significant stimulation-dependent expression changes observed in WT cells (Figures 4E and 4F). Therefore, we conclude that the shift in *HDAC7* alternative splicing toward iE9 upon stimulation results in increased sequestration of HDAC7 by 14-3-3 proteins, which, in turn, drives many changes in gene expression through changing hPTMs. We note that we also detect approximately 100 genes that exhibit alternative splicing in the ΔE9 and/or iE9 cells compared with WT (Data S2), none of which overlap with the genes that display changes in expression in the CRISPR-modified cell lines. While we have not pursued the splicing observations further, our data are consistent with previous studies demonstrating changes in splicing resulting from changes in epigenetic marks.[2,3,9]

HDAC7 protein isoforms differentially regulate expression of T cell surface markers

Importantly, GO of the DEGs in iE9 cells vs. WT and ΔE9 revealed that the top five GO biological processes (BPs) represented in these DEGs are iterations of T cell activation and cell migration/adhesion (Figure 5A). Analogously, enriched GO cellular component (CC) categories include cell surface and plasma membrane components (Figure 5A), while molecular functions (MFs) include cytokine and chemokines, as well as signal transduction (Figure 5A). Together, these categories suggest that iE9 protein expression, and thus *HDAC7* alternative splicing, is important for proper T cell stimulation response.

Three genes that exhibit enhanced expression in iE9 cells based on the RNA-seq analysis particularly caught our attention, namely the genes that encode CD3ε, CD28, and CD69. CD3ε is a component of the TCR complex, while CD28 is a receptor for co-stimulatory signals essential for full T cell activation.[44–46] Similarly, CD69 is an early marker of T cell

activation and promotes full T cell migration and effector function.[47,48] Given the relevance of these proteins for T cell activity, we wanted to determine if the cell surface expression of these proteins was indeed under the control of HDAC7 isoform expression. qRT-PCR confirmed not only the well-described stimulation-induced expression of the genes encoding CD3ε, CD28, and CD69 but also that these genes are more highly expressed in iE9 cells compared with WT or ΔE9 (Figures 5B, 5D, and 5F). Even more strikingly, flow cytometry demonstrated a dramatic increase in cell surface expression of CD3ε, CD28, and CD69 in stimulated iE9 cells relative to WT (Figures 5C, 5E, and 5G). Further consistent with the notion that the HDAC7-iE9 isoform promotes expression of these critical cell surface proteins, we observe a decrease in CD28 and CD69 (by mean fluorescence intensity [MFI]) in the cells that lack any HDAC7-iE9 (i.e., ΔE9 cells) relative to the WT cells that express roughly equal levels of both proteins (Figures 5C and 5E), while we find that expression of iE9 alone is sufficient to induce at least some cell surface expression of CD3ε and CD69 even in the absence of stimulation (Figures 5E and 5G).

From these experiments, we conclude that HDAC7 protein isoforms differentially regulate expression of T cell activation and cell surface receptor genes. Specifically, our data suggest that inclusion of exon 9 of *HDAC7* increases expression of CD3ε, CD28, and CD69 because inclusion of exon 9 causes HDAC7 to be sequestered by 14-3-3 proteins, resulting in reduced nuclear function. A prediction of this model is that HDAC7-iE9 would be expected to phenocopy a nuclear depletion of HDAC7 (or HDAC7 knockout), while exclusion of *HDAC7-E9* would result in a protein (HDAC7-ΔE9) that retains histone deacetylation and gene repressive activity. Indeed, in cells depleted of HDAC7 through a CRISPR-induced frameshift (knockout [KO]), we observe increased expression of at least *CD28* and *CD69* (Figure S5B), as we observe in the CRISPR iE9 cells (Figure 5). Moreover, reintroduction of the HDAC7-iE9 isoform in the KO cells does not alter *CD28* and *CD69* expression, while reintroduction of the HDAC7-ΔE9 isoform reduces *CD28* and *CD69* expression relative to the KO (Figure S5B).

Finally, as further demonstration that the gene expression pattern observed in the CRISPR iE9 cells is due to loss of activity, rather than a gain of function due to overall higher HDAC7-iE9 protein levels, we treated cells with an antisense morpholino oligo (AMO) targeting the 5′ UTR of *HDAC7* to block translation and knock down protein expression to bring the level of HDAC7-iE9 to that of HDAC7-ΔE9 (Figure S6A). Importantly, reduced expression of HDAC7-iE9 does not result in any appreciable changes in CD3ε, CD28, and CD69 cell surface expression with regards to either the percentage of positive cells or the MFI (Figure S6B). Together, our data support a model of stimulation-induced changes in *HDAC7* alternative splicing driving increased association of HDAC7 with 14-3-3 proteins, resulting in sequestration of HDAC7 from histones and corresponding changes in hPTMs and expression of genes critical for T cell effector functions (see below). We (Figure S7) and others[28] have observed that the bulk of HDAC7 in WT T cells is in the cytoplasm, yet at least the ΔE9 isoform of HDAC7 does associate with histone H3 (Figure S4A). This localization and interaction data, together with the fact that gene expression in the WT and ΔE9 cells is largely similar (Figure 4C), suggests that the ΔE9 isoform has dominant repressive activity in terms of hPTMs and gene expression, and the switch to the iE9 isoform

removes or reduces this dominant activity to promote active gene transcription in stimulated cells.

HDAC7-E9 alternative splicing is regulated by CELF2 and JNK signaling and occurs in developing thymocytes

Finally, given the functional relevance of alternative inclusion of *HDAC 7* exon 9, we wanted to understand more of the mechanistic drivers of this regulation. Previous work from our lab has identified several signaling-RNA-binding protein (RBP) axes where specific signaling pathway activities modulate the splicing activity of particular RBPs during T cell stimulation.[32,49–51] We first tested which, if any, of our previously studied signaling pathways contributed to alternative splicing of *HDAC7* by inhibiting these pathways prior to stimulation of the Jurkat cells. Notably, we find that inhibition of the MAP kinase axis (PKC/JNK),[51,52] but not Akt,[49] blocks the ability of PMA to induce a change in *HDAC7* splicing (Figure 6A). We have previously shown CELF2 expression to be enhanced in a JNK-dependent manner in Jurkat cells.[51] To test if the JNK-dependent increase in CELF2 expression might contribute to the increase in *HDAC7-E9* inclusion upon stimulation, we depleted CELF2 by short hairpin RNA (shRNA). Indeed, loss of CELF2 abrogates the stimulation-induced increase in *HDAC7-E9*, while depletion of hnRNP L, another well-characterized splicing regulator in T cells that does not change in a signal-dependent manner,[53] has no impact on HDAC7 alternative splicing (Figure 6B). Further, consistent with regulation of *HDAC7* exon 9 through the JNK-CELF2 axis, analysis of putative splicing-regulatory motifs in the genomic sequences around *HDAC7* exon 9 suggest binding of CELF2 downstream of *HDAC7-E9* (Figure 6C). Notably, we and others have shown that binding of CELF2 downstream of an exon enhances its inclusion in the final message.[54,55] Therefore, association of CELF2 with its cognate binding sites downstream of *HDAC7* exon 9 is predicted to enhance *HDAC7-E9* inclusion under conditions such as JNK signaling, in which CELF2 expression is increased.

In previous work, we have shown that the PMA-/JNK-induced expression of CELF2 in our Jurkat cell model mimics an increase in CELF2 expression that is observed upon pre-TCR signaling in thymocytes.[50] In particular, we have shown there to be a doubling of *CELF2* expression between CD4/CD8 double-negative (DN) thymocytes and CD4/CD8 DP thymocytes in both mice and humans. Moreover, we have observed a difference in splicing between DN and DP thymocytes for events that are driven by CELF2 in the Jurkat cells.[32,50] Interestingly, in a previous RNA-seq study we published,[32] *HDAC7-E9* inclusion was found to increase in human DP cells relative to DN. Using total RNA from that study, we have validated this change in splicing of *HDAC7-E9* in a manner that correlates with the increase in CELF2 expression (Figure 6D). KO of HDAC7 in mouse thymocytes induces changes in gene expression that phenocopies that induced by positive selection,[27] suggesting that decreased nuclear activity of HDAC7 helps drives at least some of the gene expression changes observed between DN and DP cells. Consistently, we have validated that higher levels of *CD3, CD28*, and *CD69* expression correlates with increased inclusion of *HDAC7-E9* in our purified DP vs. DN cells (Figure 6E). Therefore, we conclude that our Jurkat cell model of *HDAC7* splicing regulation mirrors a physiologically important splicing switch in developing thymocytes in which CELF2-driven inclusion of *HDAC7-E9*

leads to increased interaction of HDAC7 with 14-3-3 proteins to sequester its activity from chromatin, resulting in increased histone acetylation and expression of genes critical to T cell signaling and development (Figure 7).

DISCUSSION

HMEs are defined as “writers” or “erasers,” which catalyze the addition or removal of covalent hPTMs, respectively.[12,13] hPTMs, in turn, have been shown in several studies to correlate with changes in alternative splicing.[4–7,57] However, much less is known about how alternative splicing of HMEs might impact the epigenetic landscape. Here we show that several genes encoding HMEs are alternatively spliced in response to cell stimulation. These splicing changes are predicted to have effects that range from N/C terminus truncations or loss/gain of functional domains to changes in UTRs that may regulate protein expression.

As a model to explore how alternative splicing of HMEs impact the epigenetic and transcriptional landscape, we focused on the regulated inclusion of exon 9 of the gene encoding HDAC7, as this protein had already been implicated in controlling transcription in response to T cell signaling and differentiation.[28] Moreover, regulated inclusion of *HDAC7-E9* is one of the largest splicing changes in HMEs we observed in response to our cell stimulation. Our data reveal that inclusion of exon 9 promotes the interaction of HDAC7 with 14-3-3 proteins, which are known to stabilize HDAC7 and sequester it in the cytoplasm. Consistently, we observe that the longer isoform of HDAC7 has increased stability and decreased interaction with histone proteins compared with the isoform that lacks exon 9 peptides. Furthermore, cells that express solely the longer isoform of HDAC7 exhibit altered epigenetic marks and gene expression compared with those that express the smaller isoform. Together, these data imply that the increased inclusion of *HDAC7-E9* that occurs upon induction of JNK signaling and CELF2 expression in stimulated cells is at least one mechanism driving increased expression of genes critical for effector T cell function such as *CD28, CD69*, and *CD3*.

Previous work with modulated HDAC7 protein expression (knockdown, overexpression) showed altered H3K9ac, H3K14ac, H3K27ac, and H4K16ac levels at specific gene promoters by chromatin IP (ChIP)-qPCR.[21,22] Specifically, Azagra et al. showed that H3K9acK14ac, H3K27ac, and H4K16ac marks increased and H3K27me3 decreased after total HDAC7 KO as measured by ChIP-qPCR at the promoter region of four HDAC7 target genes (*Itgam, Ccl3, Cd28, Cd69*). Our model of inclusion of exon 9 determining how well HDAC7 is sequestered by 14-3-3 proteins predicts that cells expressing only the longer isoform of HDAC7 would mimic HDAC7 KO in terms of histone modifications, while the converse effect would be seen in the cells expressing only the smaller isoform. Indeed, we observe higher levels of H3K9ac in cells expressing only the long isoform of HDAC7 and higher levels of H3K27 methylation in cells expressing only the smaller isoform. These data also are consistent with the increase in gene and protein expression we observe, at least for CD28 and CD69, in the iE9 cells.

While epigenetic changes driven by interaction and sequestration of HDAC7 by 14-3-3 proteins do provide a mechanism for the gene expression changes, this model does not

rule out other potential mechanisms. Notably, our MS data do show interaction of HDAC7 with several transcription factors such as MEF2D, STAT3, MAZ, and MORF4L1. While at least some of these (MEF2D) appear to interact equally well with both isoforms of HDAC7, there may be differences in the interactions beyond our limit of discrimination that impact transcriptional activity. Of note, the genes that are differentially expressed in the cells expressing solely the long isoform of HDAC7 are enriched for targets genes of the transcription factors IKZF1, MEF2D, and CTBP2, which are all known binding partners of HDAC7.[38,58] Moreover, alternative splicing of at least one other gene, that encoding Sirtuin 2 (SIRT2), has been shown to regulate interactions with 14-3-3 proteins,[59–62] suggesting that splicing may regulate the interaction of a family of proteins with 14-3-3 chaperones. In sum, alternative splicing of *HDAC7* provides an important model for how splicing can regulate protein function via altered protein-protein interactions.

Finally, beyond T cells, HDAC7 is also broadly implicated in the development of heart and muscle cells, angiogenesis, and apoptosis.[20–22,63–65] Notably, CELF2 is also tightly regulated and critical to heart and skeletal muscle development.[66–68] Therefore, the functional impact we describe for the alternative splicing of *HDAC7* in T cells is likely to also be relevant for the differentiation of other tissues.

Limitations of the study

As noted above, our data and model are consistent with other studies demonstrating that interaction with 14-3-3 increases nuclear export of HDAC7, but we acknowledge that for technical reasons, the nuclear population of HDAC7 is difficult to quantify. Therefore, we cannot rule out that the iE9 version of HDAC7 has decreased HDAC7 activity in the nucleus via mechanisms other that by 14-3-3 mediated nuclear export. Moreover, we anticipate that HDAC7 likely also has cytoplasmic activities, which may also be regulated by inclusion of exon 9; however, identifying and investigating such additional activities is beyond the scope of this study.

STAR✉METHODS

RESOURCE AVAILABILITY

Lead contact—Further information and requests for resources and reagents should be directed to and will be fulfilled by the lead contact, Kristen W Lynch (klync@pennmedicine.upenn.edu).

Materials availability—This study did not generate new unique reagents.

Data and code availability

- RNA-seq data have been deposited at GEO (GSE213373) and are publicly available as of the date of publication. Accession number is also listed in the key resources table. Proteomic data have been deposited in PRIDE (PXD036471) and are publicly available as of the date of publication. Accession number is also listed in the key resources table.
- This paper does not report original code.

- Any additional information required to reanalyze the data reported in this paper is available from the lead contact upon request.

EXPERIMENTAL MODEL AND SUBJECT DETAILS

Cell lines—Jurkat cells (JSL1 clone[52]) were cultured in RPMI 1640 (Corning: 10-040-CV) supplemented with 5% heat-inactivated fetal bovine serum (FBS; Gibco: 16,000-044), penicillin and streptomycin (100 units/mL each), and grown at 37°C in 5% CO2.

METHOD DETAILS

Cell stimulation—For stimulation of Jurkat cells, we set up independent replicates by diluting cells to ~3.5×10^5 cells/mL and treating with 20 ng/mL phorbol 12-myristate 13-acetate (PMA) for 48 h prior to cell harvest. Unstimulated JSL1 cells were cultured in parallel for each replicate at a seeding concentration of ~2.5×10^5 cells/mL. For inhibition studies, cells were pre-treated with inhibitors SP600125 (JNK, 50 μM, Calbiochem, 420,119), Gö6983 (PKC, 5 μM, Selleck, S2911), R0-31-8220 (PKC, 1 μM, Selleck, S7207), Sotrastaurin (PKC, 5 μM, Selleck, S2791), MK2206 (AKT, 5 μM, Selleck, S1078), or GDC-0068 (AKT, 1 μM, Selleck, S2808) for 1 h before stimulating as described above. Transcription inhibition was achieved by incubation of cells with actinomycin D for 0–12 h (5 μg/mL final concentration). Translation inhibition was achieved by incubation of cells with cycloheximide for 0–12 h (5 μg/mL final concentration). Expression of short hairpin RNAs (shRNAs) and cDNA expression plasmids (see Cloning and CRISPR designs and Transfections below) was achieved by pre-treating cells with doxycycline for 24 h (1 mg/mL final concentration) prior to setting up unstimulated/stimulated cultures as described above. For PMA time course experiments, cells were diluted to ~3.5×10^5 cells/mL, treated with PMA and collected at 0, 3, 6, 9, 12, 24, 36, and 48 h post-PMA treatment.

Flow cytometry—Jurkat T cells were stimulated under indicated conditions. About half a million cells per condition were harvested, washed and incubated with fluorophore-conjugated antibodies for 20 min at room temperature in MACS buffer (DBPS without calcium and magnesium, supplemented with 1% FBS). Cells were washed and resuspended in MACS buffer and analyzed by flow cytometry in corresponding fluorescent channels relative to unstained control. Antibodies used: anti-CD69 PE, anti-CD28 APC, anti-CD3 BV711, anti-CD45RO BV711, anti-CXCR3 FITC, anti-CCR4 BV421, anti-CCR6 BV605, and/or anti-CCR7 BV650 antibodies (all diluted 1:100 and from Biolegend).

Cloning and CRISPR designs—To generate HDAC7 exon 9 knock-out (ΔE9) and knock-in (iE9) clones, as well as HDAC7 total protein knock-out (by deleting exon 4 from the CDS), we used CRISPR editing to target the *HDAC7* gene in JSL1 cells. The sgRNAs were designed using the Broad Institute CRISPick tool (https://portals.broadinstitute.org/gppx/crispick/public) and cloned into the pSpCas9(BB)-2A-GFP (PX458) plasmid (Addgene, #48138) containing the S. pyogenes Cas9 (SpCas9), GFP and U6 promoter sequences. A repair template for the iE9 CRISPR scheme contains a fused exon 9–10, equivalent to what is generated post-splicing in the wildtype case. This fused exon is spliced accurately to both the upstread exon 8 and downstream exon 11 in the final mRNA expressed in the iE9 cells. The fused exon was generated by assembling

the upstream and downstream homology arm PCR amplicons (~800 base pairs each) and synthesized gBlock (lacking *in9-10* sequence, IDT) onto the pUC19 vector backbone using NEBuilder tool and HiFi DNA Assembly kit (https://nebuilder.neb.com/#!/, NEB E2621L). Guide RNA, repair template (PCR and assembly) primers are in Table S1, and gBlock sequences are provided below.

$$\text{gBlock}\left(\text{HDAC7 in8–9} \rightarrow \text{ex9} \rightarrow \text{ex10} \rightarrow \text{in10} - 11, 5^{'} \rightarrow 3^{'}\right):$$

GCAGAACAATGCGCAGGACAGGGGGACAGAGATGGGGAGGAAGGATGGGTCCAT
CCCAAGCTTGGCTCTTAGCAGGGTGCAGGGACCCAGCCCCTTCCCTGAAGAAGC
AGCAGACTCACCAGTCAGCAGCGGGGCATGAGAGCCTGAGGGGTCCAGGAGGAG
AATGGGCTGCAGGCGAGAGGGCAAGGTGCCCCCAGCCTCGGGCTCCAAGCCATG
GGGCAGGAAGAGGGGAGTGTGGGGGCTCCCCAGGATTGGCCCCCGAGGGCCCA
GAGTCGGATGGGTCCTGCGGTCACTGTCAGCCCTGGCAGGGGCGGGCAGCCCCA
GAGTGATTGCGGGCAGCAAGGACACTGTCGGCAAGGCGAACGGGGCCACAGAA
GTCTCCTGCAGCCGCAGCCGCTGGCCCAAGAGCGCCTGCCATAGGGAGCAGGGC
GAGGGTCACCGGTCCCAGACCTCTACCCCGGCGCACCTTCCCCAGAACACCC.

For exogenous HDAC7 cDNA expression, the HDAC7 (NM_015401) human ORF cDNA (991 amino acids, ^{1}MHSPGADGTQ; purchased from Origene, Rockville, MD, USA; #RC215233) was cloned into the pEFnFlag and pDoxnFlag vectors with a 5′-GGATCT-3′ spacer.[32] We further engineered the plasmids by deleting the first 39 amino acids to yield cDNA expression from a downstream translation start site to reflect the endogenous CDS in JSL1 cells (952 amino acids, ^{1}MDLRVGQRPP). HDAC7 ΔE9 vectors were generated by inserting PCR amplicons (HDAC7 ^{1}MHSPGADGTQ or ^{1}MDLRVGQRPP->exon 8 and exon 10->stop codon, 954 or 915 amino acids, respectively) into the pEFnFlag and pDoxnFlag vectors.

Transfections—All JSL1 transfections were done by electroporating 10–20 million cells. To generate HDAC7-ΔE9 cells, the pSpCas9-HDAC7 in8–9 and pSpCas9-HDAC7 in9–10 vectors described above were co-transfected into JSL1 cells (5 μg of each circularized plasmid into 10 million cells). Likewise, HDAC7-ΔE4 cells (total protein knockout) were generated by transfecting 5 μg each of pSpCas9-HDAC7 in3–4 and pSpCas9-HDAC7 in4–5 into JSL1 cells. Lastly, to generate HDAC7-iE9 cells, we co-transfected 5 μg each of pSpCas9-HDAC7 in8–9, pSpCas9-HDAC7 in10–11 and pUC19-HDAC7 in7-8->in12–13 (repair template) into JSL1 cells. Cells were allowed to recover for 2–3 days in high-serum RPMI medium (10% FBS) before positive selection of GFP expression and single-cell sorting (FACS Aria) into 96-well plates to generate single-cell clones (one or three cells per well). Single clones were expanded and screened by sequencing of genomic DNA and cDNA and by Western blot analysis of protein expression (or lack thereof for HDAC7-ΔE4 cells).

Expression of the 1XFLAG-tagged HDAC7 cDNA was achieved by stable integration of the pDoxnFlag cDNA expression constructs (described above) into JSL1 cells (10 μg of linearized plasmid into 10–20 million cells) with neomycin as a selectable marker.

Specifically, for FLAG-immunoprecipitation followed by nLC-MS/MS (see below), WT JSL1 cells were transfected with pDoxnFlag-HDAC7-iE9 (991 a.a. cDNA) or pDoxnFlag-HDAC7-ΔE9 (954 a.a. cDNA). For FLAG-immunoprecipitation followed by Western blot experiments, HDAC7-ΔE4 cells were transfected with pDoxnFlag-HDAC7-iE9 (952 a.a. cDNA) or pDoxnFlag-HDAC7-ΔE9 (915 a.a. cDNA).

Protein depletion (knock-down, KD) of RNA binding proteins (RBPs) CELF2 and HNRNPL was done by stable integration of the lentivirus shRNAs into JSL1 cells (10 mg of linearized plasmid into 10–20 million cells) with neomycin as a selectable marker.[32,73]

Lastly, JSL1 cells (10 million) were transfected with 0 or 10 nmol of antisense morpholino oligo (AMO; GeneTools) to induce skipping of *HDAC7-E9* (target: *E9* 5′ splice site), HDAC7 protein knock-down (target: *HDAC7* 5′UTR target) or a negative control (target: *HDAC7* exon 2 5′ splice site). AMO sequences listed in the key resource table. Cells were incubated with AMO for 24 h after transfection and then stimulated with PMA as described above.

RNA-seq of CRISPR cell lines—Wild-type JSL1 (one clone) and CRISPR cells (HDAC7-iE9, one clone; HDAC7-ΔE9, three clones) were incubated for 48 h −/+ PMA (see above). Total RNA was extracted using RNA-STAT (Tel-Test, Inc.). RNA quality was assessed using a Nanodrop and Agilent 2100 Bioanalyzer. Samples were required to have a 260/280 ratio of >1.8 as well as a RIN value of >6 to be used for library preparation. Poly(A) selected cDNA libraries were generated on site at Genewiz (now Azenta Life Sciences, NJ, USA) using standard methods. cDNA libraries were then sequenced for paired-end, 150-nt, reads on an Illumina HiSeq (16 samples total, ~350 million raw paired-end reads, ~25 million reads per sample). Data is publicly available at GEO: GSE213373. Raw reads were aligned to the human genome (hg38) using STAR.[69]

RT-PCR—Low-cycle reverse transcription (RT)-PCR analysis of alternative splicing events were performed according to standard methods.[52,74] Primer sequences and RT-PCR conditions are provided in Table S1. In brief, we isolated RNA form unstimulated or stimulated cells using RNA-STAT (Tel-Test, Inc.) and reverse transcribed (RT) the RNA using MMLV RT (28025013; Thermo) and sequence-specific primers. We set-up three independent RT-PCR reactions with 0.5 μg of RNA and used formamide buffer to run samples on 5% denaturing polyacrylamide gels (PAGE). Lastly, we detected the 32P labeled cDNA products by densitometry using a Typhoon PhosphorImager (Amersham Biosciences) and quantified product bands with ImageQuant software.

RT-qPCR—RNA samples (0.5 μg) were reverse transcribed using MMLV RT (Thermo, 28025013) and sequence-specific primers for individual genes (Actin, CD28, CD69, HDAC7). Diluted cDNA (1:10) was used for SYBR-based quantitative (q)PCR (Applied Biosystems, 4368577) in an Applied Biosystems QuantStudio 6 Flex system and a 384-well plate format. Relative quantification was calculated according to the ΔΔCT method.[75] Significance was determined using one-way ANOVA. Primer sequences are listed in Table S1.

Western blot—For protein analysis, 5–30 μg of whole cell protein extract (WCE) were loaded into 6%–15% 37.5:1 bis-acrylamide SDS-PAGE gels, depending on protein of interest size. Antibodies for Western blot were diluted in 5% BSA-TBST as follows: HDAC7 (Cell Signaling D4E1L, 1:1000), Lamin-B1 (Abcam ab133741; 1:5000), PKM2 (Cell Signaling D78A4; 1:1000), Flag (Cell Signaling, 1:1000-2000), pan histone H3 (Abcam ab1791), H3K9ac (Abcam ab4441), H3K27ac (Abcam ab4729), HNRNPL (4D11, Abcam ab6106).

FLAG immunoprecipitation—Whole cell extract from doxycycline-treated pDoxnFlag-HDAC7 iE9/ΔE9 stable cells and WT JSL1 cells (−/+ 48 h of PMA) were generated using FLAG lysis buffer (50 mM Tris HCl, pH 7.4, 150 mM NaCl, 1 mM EDTA, 1% Triton X-100, 1X cOmplete Protease Inhibitor Cocktail (Roche)). Lysates were treated with micrococcal nuclease (MNase, NEB, M0247S) for 30 min at 37°C. Protein concentration was determined by Bradford assay (Bio-Rad: 500-0006). For immunoprecipitation (IP), 500 μg of protein were incubated with 40 μL of EZ view red ANTI-FLAG M2 affinity gel beads (Sigma, F2426) according to manufacturer's protocol (overnight at 4°C with continuous rotation, total volume 1 mL). Beads were washed at least three times with 1mL of Sigma wash buffer and samples were eluted using 2X SDS-PAGE sample buffer (62.5mM Tris HCl, pH 6.8 with 2% SDS, 10% (v/v) glycerol and 0.002% bromophenol blue).

IP sample processing and nanoLC-MS/MS—We generated three independent replicates for each IP, including wild-type JSL1 cells for a negative control. Proteins were denatured (10 mM DTT, 30 min, 55°C), alkylated (25 mM iodoacetamide, 30 min, room temperature), and digested on-beads overnight at 37°C using 2 μL of trypsin (Promega, Fisher Scientific: PRV5113; buffer: 50 mM ammonium bicarbonate). Samples were centrifuged and supernatant was transferred to new tubes, dried in a Speedvac and resuspended in 0.1% TFA for stage-tipping. C18 stage-tips were equilibrated with 100 μL of 0.1% TFA, applied with sample, and washed once with 100 μL 0.1% FA. Elution of peptides was performed by using 50 μL of 70% acetonitrile +0.1% FA (twice). Samples were dried on a Speedvac and resuspended in 0.1% TFA for subsequent nano liquid chromatography coupled to tandem mass spectrometry (nanoLC-MS/MS) analysis.

Samples were analyzed by using an EASY-nLC nano high-performance liquid chromatography (HPLC) system (Thermo Scientific, Sn Jose, CA, USA) coupled online with a Fusion Orbitrap Tribrid mass spectrometer instrument (Thermo Scientific, San Jose, CA, USA). NanoLC was configured with a 75 μm ID x 20 cm Reprosil-Pur C18-AQ (3 μm; Dr. Maisch GmbH, Germany) reverse phase capillary column packed in-house. The full HPLC method was 135 min long with a 125 min gradient as detailed: 1%–28% solvent B (solvent A = 0.1%formic acid; solvent B = 0.1% formic acid in 100% acetonitrile) over 120 min and from 28% to 90% solvent B in 5 min at a flow-rate of 300 nL/min. Data were acquired using data-dependent acquisition (DDA) and positive polarity modes, consisting on a full scan MS spectrum (350–1200 m/z) performed in the orbitrap at 120,000 resolution (cycle time = 3 s), followed by collision induced dissociation (CID) fragmentation of the precursor ions (2–6 charge state, intensity threshold minimum = 2 × 10e4). CID collision

energy was set at 30. MS/MS scans detected on the ion trap (AGC target minimum = 1 × 104). Xcalibur software was used for data collection.

Histone PTM analysis—Cells were collected by centrifugation, washed in PBS and stored at −80°C until further analysis. At least three biological replicates were used for each condition. Histone extraction and digestion was carried out according to standard procedures.[39] Briefly, nuclei were isolated by suspension of cells in 10X volume of nuclear isolation buffer (15 mM Tris-HCl pH = 7.5, 60 mM KCl, 15 mM NaCl, 5 mM MgCl2, 1 mM CaCl2 and 250 mM sucrose, 0.2% NP-40) with 1 mM DTT, 5 nM microcystin, 0.5 mM ASBSF and 10 mM sodium butyrate on ice. Nuclei were pelleted by centrifugation at 1000 g for 5 min at 4 °C and washed twice with nuclear isolation buffer in the absence of NP-40. To the pelleted nuclei, 0.4 N H2SO4 was added to a final ratio of 5:1 and incubated for 2–4 h with shaking at 4 °C. Samples were centrifuged at 3400 g for 10 min at 4 °C and the supernatants were collected and incubated on ice with ¼ volume of 100% TCA for 1 h. Precipitated histones were collected by centrifugation at 3400 g for 10 min at 4 °C and pellets were rinsed once with ice-cold acetone containing 0.1% HCl and once with ice-cold acetone. Protein concentration was determined using a Bradford assay. For MS analyses of histone PTMs, ~40 μg of histones were resuspended in 20 μL of 50 mM ammonium bicarbonate and subjected to derivatization with propionic anhydride, digested with trypsin for 6 h at 37 °C and desalted with C18 stage-tips as described above.

About 2 μg of peptides were injected into a 75 μm ID x 20 cm Reprosil-Pur C18-AQ (3 μm; Dr. Maisch GmbH, Germany) nano-column (packed in-house) using an EASY-nLC nano HPLC (Thermo Scientific, Odense, Denmark). The mobile phases consisted of water with 0.1% (v/v) formic acid (A) and acetonitrile with 0.1% (v/v) formic acid (B). Peptides were eluted using a gradient of 0–26% B over 45 min followed by 26–98% B over 5 min and maintained for 10 min at 300 nL per min. The nano HPLC was coupled to a Q Exactive or an Orbitrap Fusion mass spectrometer (Thermo Scientific, San Jose, California). Spray voltage was set at 2.4 kV and capillary temperature was set at 275°C. For DIA, a full scan MS spectrum (m/z 300–1,100) was acquired in the Orbitrap with a resolution of 120,000 (at 200 m/z) and an AGC target of 5 × 105 or in the ion trap with an AGC target of 3 × 104. MS/MS was performed with an AGC target of 3 × 104 using an injection time limit of 30 or 60 ms. All acquisitions were performed in positive mode polarity.

QUANTIFICATION AND STATISTICAL ANALYSIS

RNA-seq computational analyses—Differential gene expression of transcripts was performed using the R package DESeq2.[70] Significantly changing genes were defined as those with a log2 fold change > |2|, a corresponding adjusted p value <0.05 and baseMean TPM ≥20. Differential splicing analysis was performed using rMATS.[71,72] Significantly changing skipped exon events were defined as those with an inclusion level difference ≥|0.2|, FDR ≤0.05 and reads ≥10 (for both exon inclusion/skipped isoforms). Gene Ontology (GO) analyses were performed using the ShinyGO tool (v0.741, [33]). We selected the top, non-redundant significant categories with an FDR q-value <0.05 and enrichment score >2.

To identify histone modifying enzyme genes undergoing alternative splicing, we utilized publicly available RNA-seq data and differential splicing analysis by MAJIQ ([30], GEO: GSE93594). In brief, total RNA was isolated and poly (A) selected from unstimulated and PMA stimulated JSL1 cells using RNA-Bee (Tel-Test) according to the manufacturer protocol.[76] RNA-Seq data was analyzed with MAJIQ to identify local splice variations (LSVs) and quantify changes in exonic splicing patterns between our conditions, which we term ΔPSI (difference in percent spliced in).[31] We applied the following filters to MAJIQ identifications to compare LSVs between unstimulated and PMA stimulated JSL1 cells: ΔPSI ≥ |20%|, FDR ≤0.05 and reads ≥10. Gene Ontology (GO) analyses were performed using the ShinyGO tool (v0.741, [33]). We selected the top, non-redundant significant categories with an FDR q-value <0.05 and enrichment score >2.

Analysis of mass spectrometry data—Analysis of protein abundance was performed using the Sequest HT search engine in Proteome Discoverer 2.2 (PD 2.2, Thermo Scientific) and the Swissprot human proteome database (canonical isoforms, release 2018_05). Data has been deposited in PRIDE under project accession number PXD036471.

Analysis of histone PTMs was performed using our in-house software EpiProfile 2.0 with a 10-ppm tolerance for extracting peak areas from raw files.[40] The relative abundances of PTMs were calculated by dividing the intensity the modified peptide by the sum of all modified and unmodified peptides sharing the same sequence, across all detectable charge states.

Additional statistical analysis—Significance for gene, isoform and protein expression analysis using RT-PCR, qPCR and Western blots were determined using a one-way ANOVA test or Student paired t test (specified for each figure). In all cases statistics were calculated using GraphPad PRISM (http://www.graphpad.com/guides/prism/7/statistics/index.htm) and number of replicates is provided in each figure. Significance of fold enrichment for GO analysis was calculated by ShinyGO.[33]

Supplementary Material

Refer to Web version on PubMed Central for supplementary material.

ACKNOWLEDGMENTS

The authors thank Rakesh Chatrikhi for the design of ΔE9 CRISPR gRNAs; Corrinn Lucotch and H. Claire Woodward for help with RT-PCR; Shelley Berger and Roberto Bonasio for access to MS; and Sara Cherry, Ben Black, Ronen Marmorstein, and Manuel Ares for many helpful discussions. This work was supported by an NSF predoctoral fellowship to L.M.A., NIH P01 CA196539 to B.A.G., and NIH R35 GM118048 to K.W.L. All data are publicly available at GEO: GSE213373 and PRIDE: PXD036471.

REFERENCES

1. Blencowe BJ (2006). Alternative splicing: new insights from global analyses. Cell 126, 37–47. 10.1016/j.cell.2006.06.023. [PubMed: 16839875]
2. Luco RF, Allo M, Schor IE, Kornblihtt AR, and Misteli T (2011). Epigenetics in alternative pre-mRNA splicing. Cell 144, 16–26. 10.1016/j.cell.2010.11.056. [PubMed: 21215366]

3. Zhang J, Zhang YZ, Jiang J, and Duan CG (2020). The crosstalk between epigenetic mechanisms and alternative RNA processing regulation. Front. Genet 11, 998. 10.3389/fgene.2020.00998. [PubMed: 32973889]
4. Sahu SK, Agirre E, Inayatullah M, Mahesh A, Tiwari N, Lavin DP, Singh A, Strand S, Diken M, Luco RF, et al. (2022).A complex epigenome-splicing crosstalk governs epithelial-to-mesenchymal transition in metastasis and brain development. Nat. Cell Biol 24, 1265–1277. 10.1038/s41556-022-00971-3. [PubMed: 35941369]
5. Segelle A, Núñez-Álvarez Y, Oldfield AJ, Webb KM, Voigt P, and Luco RF (2022). Histone marks regulate the epithelial-to-mesenchymal transition via alternative splicing. Cell Rep. 38, 110357. 10.1016/j.celrep.2022.110357. [PubMed: 35172149]
6. Agirre E, Oldfield AJ, Bellora N, Segelle A, and Luco RF (2021). Splicing-associated chromatin signatures: a combinatorial and position-dependent role for histone marks in splicing definition. Nat. Commun 12, 682. 10.1038/s41467-021-20979-x. [PubMed: 33514745]
7. Luco RF, Pan Q, Tominaga K, Blencowe BJ, Pereira-Smith OM, and Misteli T (2010). Regulation of alternative splicing by histone modifications. Science 327, 996–1000. 10.1126/science.1184208. [PubMed: 20133523]
8. Fong N, Kim H, Zhou Y, Ji X, Qiu J, Saldi T, Diener K, Jones K, Fu XD, and Bentley DL (2014). Pre-mRNA splicing is facilitated by an optimal RNA polymerase II elongation rate. Genes Dev. 28, 2663–2676. 10.1101/gad.252106.114. [PubMed: 25452276]
9. Herzel L, Ottoz DSM, Alpert T, and Neugebauer KM (2017). Splicing and transcription touch base: co-transcriptional spliceosome assembly and function. Nat. Rev. Mol. Cell Biol 18, 637–650. 10.1038/nrm.2017.63. [PubMed: 28792005]
10. Fiszbein A, Giono LE, Quaglino A, Berardino BG, Sigaut L, von Bilderling C, Schor IE, Steinberg JHE, Rossi M, Pietrasanta LI, et al. (2016). Alternative splicing of G9a regulates neuronal differentiation. Cell Rep. 14, 2797–2808. 10.1016/j.celrep.2016.02.063. [PubMed: 26997278]
11. Mauger O, Klinck R, Chabot B, Muchardt C, Allemand E, and Batsché E (2015). Alternative splicing regulates the expression of G9A and SUV39H2 methyltransferases, and dramatically changes SUV39H2 functions. Nucleic Acids Res. 43, 1869–1882. 10.1093/nar/gkv013. [PubMed: 25605796]
12. Gillette TG, and Hill JA (2015). Readers, writers, and erasers. Circ. Res 116, 1245–1253. 10.1161/circresaha.116.303630. [PubMed: 25814685]
13. Yun M, Wu J, Workman JL, and Li B (2011). Readers of histone modifications. Cell Res. 21, 564–578. 10.1038/cr.2011.42. [PubMed: 21423274]
14. Downes M, Ordentlich P, Kao H-Y, Alvarez JG, and Evans RM (2000). Identification of a nuclear domain with deacetylase activity. Proc. Natl. Acad. Sci. USA 97, 10330–10335. 10.1073/pnas.97.19.10330. [PubMed: 10984530]
15. Fischle W, Kiermer V, Dequiedt F, and Verdin E (2001). The emerging role of class II histone deacetylases. Biochem. Cell. Biol 79, 337–348. 10.1139/o01-116. [PubMed: 11467747]
16. Han A, He J, Wu Y, Liu JO, and Chen L (2005). Mechanism of recruitment of class II histone deacetylases by myocyte enhancer factor-2. J. Mol. Biol 345, 91–102. 10.1016/j.jmb.2004.10.033. [PubMed: 15567413]
17. Kao HY, Downes M, Ordentlich P, and Evans RM (2000). Isolation of a novel histone deacetylase reveals that class I and class II deacetylases promote SMRT-mediated repression. Genes Dev. 14, 55–66. [PubMed: 10640276]
18. Martin M, Kettmann R, and Dequiedt F (2007). Class IIa histone deacetylases: regulating the regulators. Oncogene 26, 5450–5467. 10.1038/sj.onc.1210613. [PubMed: 17694086]
19. Parra M, and Verdin E (2010). Regulatory signal transduction pathways for class IIa histone deacetylases. Curr. Opin. Pharmacol 10, 454–460. 10.1016/j.coph.2010.04.004. [PubMed: 20447866]
20. Dequiedt F, Kasler H, Fischle W, Kiermer V, Weinstein M, Herndier BG, and Verdin E (2003). HDAC7, a thymus-specific class II histone deacetylase, regulates Nur77 transcription and TCR-mediated apoptosis. Immunity 18, 687–698. 10.1016/s1074-7613(03)00109-2. [PubMed: 12753745]

21. Azagra A, Román-González L, Collazo O, Rodríguez-Ubreva J, de Yebenes VG, Barneda-Zahonero B, Rodríguez J, Castro de Moura M, Grego-Bessa J, Fernández-Duran I, et al. (2016). In vivo conditional deletion of HDAC7 reveals its requirement to establish proper B lymphocyte identity and development. J. Exp. Med 213, 2591–2601. 10.1084/jem.20150821. [PubMed: 27810920]
22. Barneda-Zahonero B, Collazo O, Azagra A, Fernández-Duran I, Serra-Musach J, Islam ABMMK, Vega-García N, Malatesta R, Cameos M, Gómez A, et al. (2015). The transcriptional repressor HDAC7 promotes apoptosis and c-Myc downregulation in particular types of leukemia and lymphoma. Cell Death Dis. 6, e1635. 10.1038/cddis.2014.594. [PubMed: 25675295]
23. Barneda-Zahonero B, Román-González L, Collazo O, Rafati H, Islam ABMMK, Bussmann LH, di Tullio A, De Andres L, Graf T, López-Bigas N, et al. (2013). HDAC7 is a repressor of myeloid genes whose downregulation is required for transdifferentiation of pre-B cells into macrophages. PLoS Genet. 9, e1003503. 10.1371/journal.pgen.1003503. [PubMed: 23696748]
24. Dequiedt F, Van Lint J, Lecomte E, Van Duppen V, Seufferlein T, Vandenheede JR, Wattiez R, and Kettmann R (2005). Phosphorylation of histone deacetylase 7 by protein kinase D mediates T cell receptor-induced Nur77 expression and apoptosis. J. Exp. Med 201, 793–804. 10.1084/jem.20042034. [PubMed: 15738054]
25. Kasler HG, Lim HW, Mottet D, Collins AM, Lee IS, and Verdin E (2012). Nuclear export of histone deacetylase 7 during thymic selection is required for immune self-tolerance. EMBO J. 31, 4453–4465. 10.1038/emboj.2012.295. [PubMed: 23103766]
26. Kasler HG, and Verdin E (2007). Histone deacetylase 7 functions as a key regulator of genes involved in both positive and negative selection of thymocytes. Mol. Cell Biol 27, 5184–5200. 10.1128/MCB.02091-06. [PubMed: 17470548]
27. Kasler HG, Young BD, Mottet D, Lim HW, Collins AM, Olson EN, and Verdin E (2011). Histone deacetylase 7 regulates cell survival and TCR signaling in CD4/CD8 double-positive thymocytes. J. Immunol 186, 4782–4793. 10.4049/jimmunol.1001179. [PubMed: 21398603]
28. Myers DR, Lau T, Markegard E, Lim HW, Kasler H, Zhu M, Barczak A, Huizar JP, Zikherman J, Erle DJ, et al. (2017). Tonic LAT-HDAC7 signals sustain Nur77 and Irf4 expression to tune naive CD4T cells. Cell Rep. 19, 1558–1571. 10.1016/j.celrep.2017.04.076. [PubMed: 28538176]
29. Agosto LM, Gazzara MR, Radens CM, Sidoli S, Baeza J, Garcia BA, and Lynch KW (2019). Deep profiling and custom databases improve detection of proteoforms generated by alternative splicing. Genome Res. 29, 2046–2055. 10.1101/gr.248435.119. [PubMed: 31727681]
30. Gazzara MR, Mallory MJ, Roytenberg R, Lindberg JP, Jha A, Lynch KW, and Barash Y (2017). Ancient antagonism between CELF and RBFOX families tunes mRNA splicing outcomes. Genome Res. 27, 1360–1370. 10.1101/gr.220517.117. [PubMed: 28512194]
31. Vaquero-Garcia J, Barrera A, Gazzara MR, González-Vallinas J, Lahens NF, Hogenesch JB, Lynch KW, and Barash Y (2016). A new view of transcriptome complexity and regulation through the lens of local splicing variations. Elife 5, e11752. 10.7554/eLife.11752. [PubMed: 26829591]
32. Mallory MJ, Allon SJ, Qiu J, Gazzara MR, Tapescu I, Martinez NM, Fu XD, and Lynch KW (2015). Induced transcription and stability of CELF2 mRNA drives widespread alternative splicing during T-cell signaling. Proc. Natl. Acad. Sci. USA 112, E2139–E2148. 10.1073/pnas.1423695112. [PubMed: 25870297]
33. Ge SX, Jung D, and Yao R (2020). ShinyGO: a graphical gene-set enrichment tool for animals and plants. Bioinformatics 36, 2628–2629. 10.1093/bioinformatics/btz931. [PubMed: 31882993]
34. Mallory MJ, McClory SP, Chatrikhi R, Gazzara MR, Ontiveros RJ, and Lynch KW (2020). Reciprocal regulation of hnRNP C and CELF2 through translation and transcription tunes splicing activity in T cells. Nucleic Acids Res. 48, 5710–5719. 10.1093/nar/gkaa295. [PubMed: 32338744]
35. Kosugi S, Yanagawa H, Terauchi R, and Tabata S (2014). NESmapper: accurate prediction of leucine-rich nuclearexport signals using activity-based profiles. PLoS Comput. Biol 10, e1003841. 10.1371/journal.pcbi.1003841. [PubMed: 25233087]
36. Gao C, Liu Y, Lam M, and Kao HY (2010). Histone deacetylase 7 (HDAC7) regulates myocyte migration and differentiation. Biochim. Biophys. Acta 1803, 1186–1197. 10.1016/j.bbamcr.2010.06.008. [PubMed: 20621129]

37. Li X, Song S, Liu Y, Ko SH, and Kao HY (2004). Phosphorylation of the histone deacetylase 7 modulates its stability and association with 14-3-3 proteins. J. Biol. Chem 279, 34201–34208. 10.1074/jbc.M405179200. [PubMed: 15166223]
38. Dressel U, Bailey PJ, Wang SC, Downes M, Evans RM, and Muscat GE (2001). A dynamic role for HDAC7 in MEF2-mediated muscle differentiation. J. Biol. Chem 276, 17007–17013. 10.1074/jbc.M101508200. [PubMed: 11279209]
39. Sidoli S, Bhanu NV, Karch KR, Wang X, and Garcia BA (2016). Complete Workflow for analysis of histone post-translational modifications using bottom-up mass spectrometry: from histone extraction to data analysis. J. Vis. Exp 10.3791/54112.
40. Yuan ZF, Sidoli S, Marchione DM, Simithy J, Janssen KA, Szurgot MR, and Garcia BA (2018). EpiProfile 2.0: a computational platform for processing epi-proteomics mass spectrometry data. J. Proteome Res 17, 2533–2541. 10.1021/acs.jproteome.8b00133. [PubMed: 29790754]
41. Lin-Shiao E, Lan Y, Coradin M, Anderson A, Donahue G, Simpson CL, Sen P, Saffie R, Busino L, Garcia BA, et al. (2018). KMT2D regulates p63 target enhancers to coordinate epithelial homeostasis. Genes Dev. 32, 181–193. 10.1101/gad.306241.117. [PubMed: 29440247]
42. Sen P, Lan Y, Li CY, Sidoli S, Donahue G, Dou Z, Frederick B, Chen Q, Luense LJ, Garcia BA, et al. (2019). Histone acetyltransferase p300 induces de novo super-enhancers to drive cellular senescence. Mol. Cell 73, 684–698.e8. 10.1016/j.molcel.2019.01.021. [PubMed: 30773298]
43. Bannister AJ, and Kouzarides T (2011). Regulation of chromatin by histone modifications. Cell Res. 21, 381–395. 10.1038/cr.2011.22. [PubMed: 21321607]
44. Boise LH, Minn AJ, Noel PJ, June CH, Accavitti MA, Lindsten T, and Thompson CB (1995). CD28 costimulation can promote T cell survival by enhancing the expression of Bcl-XL. Immunity 3, 87–98. 10.1016/1074-7613(95)90161-2. [PubMed: 7621080]
45. Esensten JH, Helou YA, Chopra G, Weiss A, and Bluestone JA (2016). CD28 costimulation: from mechanism to therapy. Immunity 44, 973–988. 10.1016/j.immuni.2016.04.020. [PubMed: 27192564]
46. Krummel MF, and Allison JP (1995). CD28 and CTLA-4 have opposing effects on the response of T cells to stimulation. J. Exp. Med 182, 459–465. [PubMed: 7543139]
47. D'Ambrosio D, Cantrell DA, Frati L, Santoni A, and Testi R (1994). Involvement of p21ras activation in T cell CD69 expression. Eur. J. Immunol 24, 616–620. [PubMed: 7907294]
48. Cibrián D, and Sánchez-Madrid F (2017). CD69: from activation marker to metabolic gatekeeper. Eur. J. Immunol 47, 946–953. 10.1002/eji.201646837. [PubMed: 28475283]
49. Heyd F, and Lynch KW (2010). Phosphorylation-dependent regulation of PSF by GSK3 controls CD45 alternative splicing. Mol. Cell 40, 126–137. 10.1016/j.molcel.2010.09.013. [PubMed: 20932480]
50. Mallory MJ, Jackson J, Weber B, Chi A, Heyd F, and Lynch KW (2011). Signal- and development-dependent alternative splicing of LEF1 in T cells is controlled by CELF2. Mol. Cell Biol 31, 2184–2195. 10.1128/MCB.05170-11. [PubMed: 21444716]
51. Martinez NM, Agosto L, Qiu J, Mallory MJ, Gazzara MR, Barash Y, Fu XD, and Lynch KW (2015). Widespread JNK-dependent alternative splicing induces a positive feedback loop through CELF2-mediated regulation of MKK7 during T-cell activation. Genes Dev. 29, 2054–2066. 10.1101/gad.267245.115. [PubMed: 26443849]
52. Lynch KW, and Weiss A (2000). A model system for activation-induced alternative splicing of CD45 pre-mRNA in T cells implicates protein kinase C and Ras. Mol. Cell Biol 20, 70–80. 10.1128/mcb.20.1.70-80.2000. [PubMed: 10594010]
53. Topp JD, Jackson J, Melton AA, and Lynch KW (2008). A cell-based screen for splicing regulators identifies hnRNP LL as a distinct signal-induced repressor of CD45 variable exon 4. Rna 14, 2038–2049, rna.1212008 [pii]. 10.1261/rna.1212008. [PubMed: 18719244]
54. Ajith S, Gazzara MR, Cole BS, Shankarling G, Martinez NM, Mallory MJ, and Lynch KW (2016). Position-dependent activity of CELF2 in the regulation of splicing and implications for signal-responsive regulation in T cells. RNA Biol. 13, 569–581. 10.1080/15476286.2016.1176663. [PubMed: 27096301]

55. Goo YH, and Cooper TA (2009). CUGBP2 directly interacts with U2 17S snRNP components and promotes U2 snRNA binding to cardiac troponin T pre-mRNA. Nucleic Acids Res. 37, 4275–4286, gkp346 [pii]. 10.1093/nar/gkp346. [PubMed: 19443441]
56. Gazzara MR, Vaquero-Garcia J, Lynch KW, and Barash Y (2014). In silico to in vivo splicing analysis using splicing code models. Methods 67, 3–12. S1046-2023(13)00444-1 [pii]10.1016/j.ymeth.2013.11.006 [PubMed: 24321485]
57. Hu Q, Greene CS, and Heller EA (2020). Specific histone modifications associate with alternative exon selection during mammalian development. Nucleic Acids Res. 48, 4709–4724. 10.1093/nar/gkaa248. [PubMed: 32319526]
58. Kao HY, Verdel A, Tsai CC, Simon C, Juguilon H, and Khochbin S (2001). Mechanism for nucleocytoplasmic shuttling of histone deacetylase 7. J. Biol. Chem 276, 47496–47507. 10.1074/jbc.M107631200. [PubMed: 11585834]
59. Pereira JM, Chevalier C, Chaze T, Gianetto Q, Impens F, Matondo M, Cossart P, and Hamon MA (2018). Infection reveals a modification of SIRT2 critical for chromatin association. Cell Rep. 23, 1124–1137. 10.1016/j.celrep.2018.03.116. [PubMed: 29694890]
60. Piracha ZZ, Saeed U, Kim J, Kwon H, Chwae Y-J, Lee HW, Lim JH, Park S, Shin H-J, and Kim K (2020). An alternatively spliced Sirtuin 2 isoform 5 inhibits hepatitis B virus replication from cccDNA by repressing epigenetic modifications made by histone lysine methyltransferases. J. Virol 94, e00926-20–e00920. 10.1128/jvi.00926-20. [PubMed: 32493816]
61. Rack JGM, VanLinden MR, Lutter T, Aasland R, and Ziegler M (2014). Constitutive nuclear localization of an alternatively spliced sirtuin-2 isoform. J. Mol. Biol 426, 1677–1691. 10.1016/j.jmb.2013.10.027. [PubMed: 24177535]
62. Zhu H, Zhao L, Wang E, Dimova N, Liu G, Feng Y, and Cambi F (2012). The QKI-PLP pathway controls SIRT2 abundance in CNS myelin. Glia 60, 69–82. 10.1002/glia.21248. [PubMed: 21948283]
63. Beharry AW, and Judge AR (2015). Differential expression of HDAC and HAT genes in atrophying skeletal muscle. Muscle Nerve 52, 1098–1101. 10.1002/mus.24912. [PubMed: 26372908]
64. Margariti A, Xiao Q, Zampetaki A, Zhang Z, Li H, Martin D, Hu Y, Zeng L, and Xu Q (2009). Splicing of HDAC7 modulates the SRF-myocardin complex during stem-cell differentiation towards smooth muscle cells. J. Cell Sci 122, 460–470. 10.1242/jcs.034850. [PubMed: 19174469]
65. Zhou B, Margariti A, Zeng L, Habi O, Xiao Q, Martin D, Wang G, Hu Y, Wang X, and Xu Q (2011). Splicing of histone deacetylase 7 modulates smooth muscle cell proliferation and neointima formation through nuclear β-catenin translocation. Arterioscler. Thromb. Vasc. Biol 31, 2676–2684. 10.1161/atvbaha.111.230888. [PubMed: 21836063]
66. Giudice J, and Cooper TA (2014). RNA-binding proteins in heart development. Adv. Exp. Med. Biol 825, 389–429. 10.1007/978-1-4939-1221-6_11. [PubMed: 25201112]
67. Kalsotra A, Xiao X, Ward AJ, Castle JC, Johnson JM, Burge CB, and Cooper TA (2008). A postnatal switch of CELF and MBNL proteins reprograms alternative splicing in the developing heart. Proc. Natl. Acad. Sci. USA 105, 20333–20338, 0809045105 [pii]. 10.1073/pnas.0809045105. [PubMed: 19075228]
68. Ladd AN, Charlet N, and Cooper TA (2001). The CELF family of RNA binding proteins is implicated in cell-specific and developmentally regulated alternative splicing. Mol. Cell Biol 21, 1285–1296. 10.1128/MCB.21.4.1285-1296.2001. [PubMed: 11158314]
69. Dobin A, Davis CA, Schlesinger F, Drenkow J, Zaleski C, Jha S, Batut P, Chaisson M, and Gingeras TR (2013). STAR: ultrafast universal RNA-seq aligner. Bioinformatics 29, 15–21. 10.1093/bioinformatics/bts635. [PubMed: 23104886]
70. Love MI, Huber W, and Anders S (2014). Moderated estimation of fold change and dispersion for RNA-seq data with DESeq2. Genome Biol. 15, 550. 10.1186/s13059-014-0550-8. [PubMed: 25516281]
71. Park JW, Tokheim C, Shen S, and Xing Y (2013). Identifying differential alternative splicing events from RNA sequencing data using RNASeq-MATS. Methods. Mol. Biol 1038, 171–179. 10.1007/978-1-62703-514-9_10. [PubMed: 23872975]

72. Shen S, Park JW, Huang J, Dittmar KA, Lu ZX, Zhou Q, Carstens RP, and Xing Y (2012). MATS: a Bayesian framework for flexible detection of differential alternative splicing from RNA-Seq data. Nucleic Acids Res. 40, e61. 10.1093/nar/gkr1291. [PubMed: 22266656]

73. Cole BS, Tapescu I, Allon SJ, Mallory MJ, Qiu J, Lake RJ, Fan HY, Fu XD, and Lynch KW (2015). Global analysis of physical and functional RNA targets of hnRNP L reveals distinct sequence and epigenetic features of repressed and enhanced exons. RNA 21, 2053–2066. 10.1261/rna.052969.115. [PubMed: 26437669]

74. Melton AA, Jackson J, Wang J, and Lynch KW (2007). Combinatorial control of signal-induced exon repression by hnRNP L and PSF. Mol. Cell Biol 27, 6972–6984. [PubMed: 17664280]

75. Livak KJ, and Schmittgen TD (2001). Analysis of relative gene expression data using real-time quantitative PCR and the 2(-Delta Delta C(T)) Method. Methods 25, 402–408. 10.1006/meth.2001.1262. [PubMed: 11846609]

76. Smith SA, and Lynch KW (2014). Cell-based splicing of minigenes. Methods Mol. Biol 1126, 243–255. 10.1007/978-1-62703-980-2_18. [PubMed: 24549669]

Highlights

- HDAC7 exon 9 splicing is regulated by signaling in developing and cultured T cells
- Inclusion of exon 9 promotes interaction of HDAC7 with 14-3-3 proteins
- Inclusion of HDAC7 exon 9 regulates transcription of gene targets

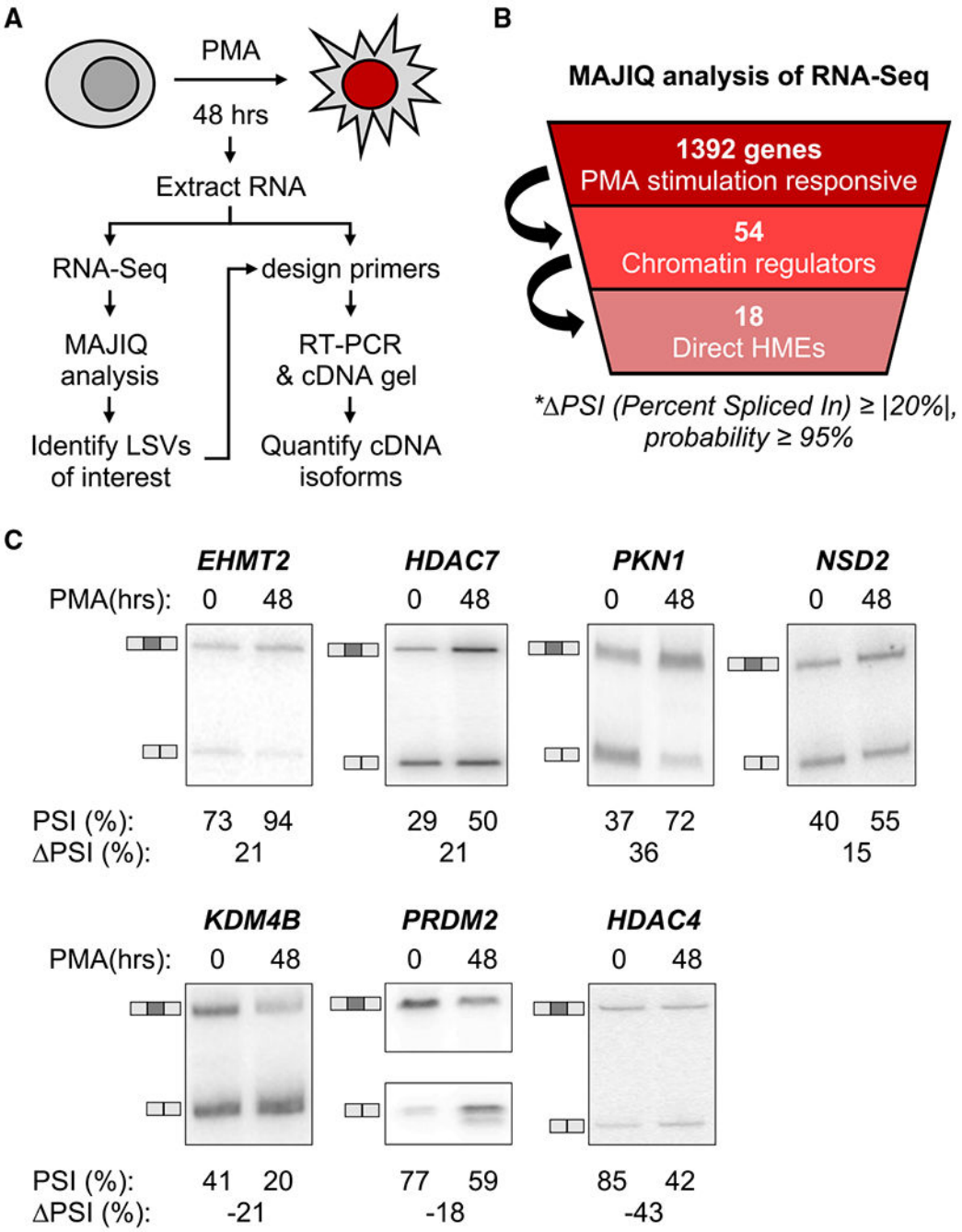

Figure 1. Identification of alternatively spliced HME genes upon T cell stimulation

(A) Workflow for identification and quantification of alternative splicing events (i.e., LSVs) using RNA-seq, MAJIQ analysis, and reverse transcription (RT)-PCR.

(B) Total number of genes with significant changes in splicing patterns upon PMA stimulation. Percent spliced in (PSI) is calculated for each condition (inclusion/skipping+inclusion products), and the difference in PSI (ΔPSI) is calculated as PSI stimulated – PSI unstimulated. Significant changes are defined as ΔPSI ≥|20%| with a probability ≥95%. HMEs, histone-modifying enzymes.

(C) Representative RT-PCR validation gels for HME alternative splicing (AS) events (PSI average and difference below gel, n = 3–4, Student's paired t test $p < 0.05$ for all). Products representing the exon skipped form are indicated by two light gray boxes indicating exons, and products representing the included form are indicated by a schematic with an additional dark gray box representing the variable exon. RT-PCR products are resolved on two gels for PRDM2 due to significant difference in size.

See also Figure S1.

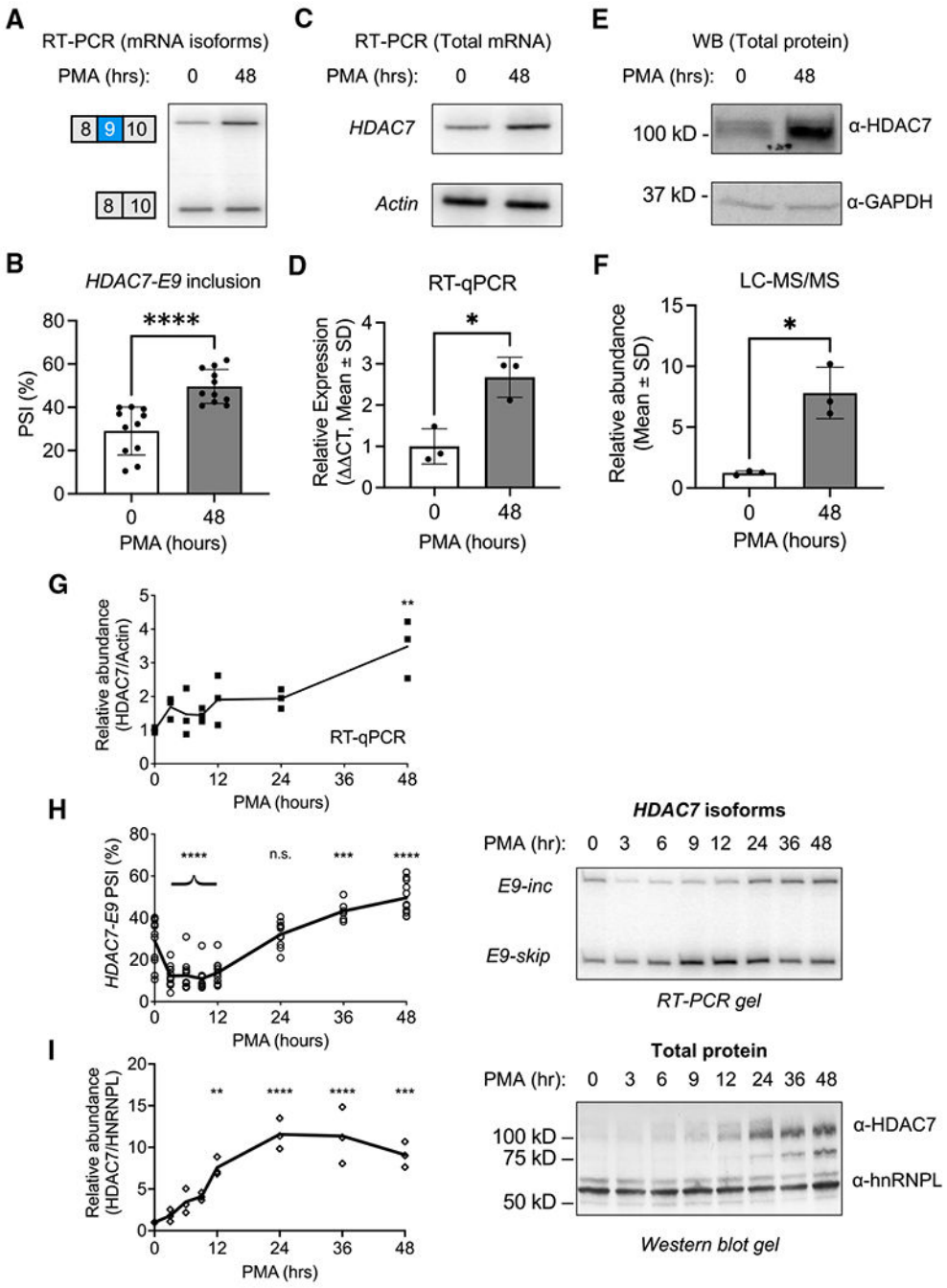

Figure 2. Increase in HDAC7 protein correlates with the increase in *HDAC7-E9* inclusion

(A and B) Representative RT-PCR gel of resolved *HDAC7* mRNA isoforms in Jurkat cells cultured with and without PMA; quantified in (B) ($n = 11$, $p < 0.0001$; bars represent the mean ± standard deviation; statistical significance determined by Student's paired t test). Products containing or lacking HDAC7 exon 9 are as indicated by the schematic.

(C and D) Representative RT-PCR of *HDAC7* and *Actin* isoforms in WT JSL1 cells; quantified by qRT-PCR and graphed in (D) ($n = 3$, $p = 0.03$; statistical significance determined by Student's paired t test).

(E) Representative western blots for HDAC7 protein with GAPDH as loading control.
(F) Quantification of HDAC7 protein using LC-MS/MS (n = 3, p = 0.03; statistical significance determined by Student's paired t test).
(G–I) PMA time course experiments in wild-type JSL1 cells (time points = 0, 3, 6, 12, 24, 36, and 48 h post-stimulation).
(G) Quantification from qPCR (n = 4, one-way ANOVA statistical test).
(H) Quantification of HDAC7 isoform expression by low-cycle radiolabeled RT-PCR (right, n = 11, one-way ANOVA statistical test). On the left is a representative gel showing products corresponding to *HDAC7* mRNAs with E9 inclusion (inc) or skipping (skip).
(I) Quantification of HDAC7 protein by western blot (right, n = 3, one-way ANOVA statistical test). On the left is a representative western blot of HDAC7 with HNRNPL as loading control.
In all cases, asterisks indicate statistical significance: *p < 0.05; **p < 0.01, ***p < 0.001, ****p < 0.0001.
See also Figure S2.

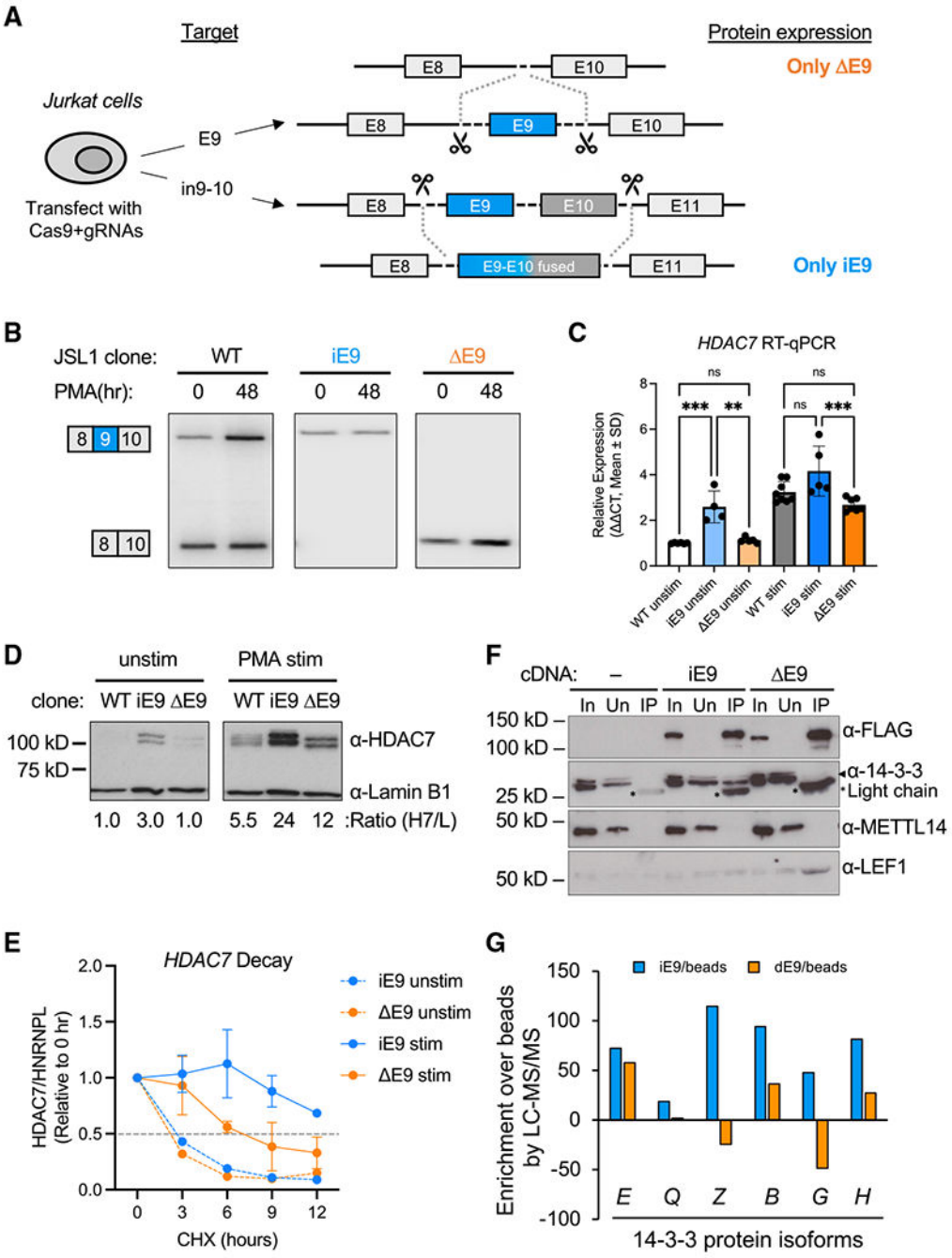

Figure 3. Inclusion of *HDAC7-E9* leads to increased HDAC7 protein expression and stability

(A) CRISPR design scheme to generate cell lines expressing single HDAC7 protein isoforms. Cells lacking exon 9 (ΔE9) generated by cutting in the introns around exon 9, while cells with forced inclusion of exon 9 (iE9) generated by using a repair template with an exon 9–10 fusion.

(B) Validation of individual CRISPR clone populations using radiolabeled RT-PCR.

(C) qRT-PCR measuring total *HDAC7* mRNA expression in WT, iE9, and ΔE9 cells under unstimulated and stimulated conditions (n = 4–8 individual replicates, one-way ANOVA statistical test).
(D) Representative western blots measuring total HDAC7 protein expression in WT, iE9, and ΔE9 cells under unstimulated and stimulated conditions. Ratios of HDAC7/lamin B1 (H7/L) signals are provided underneath each sample lane (normalized to WT).
(E) Relative expression of HDAC7 protein in iE9 and ΔE9 cells after treatment with cycloheximide (CHX) for indicated time. Relative quantification values from western blots calculated using ImageJ (unstimulated n = 1; stimulated n = 2, mean ± SEM, no statistical test performed).
(F) Protein interactors of iE9 and ΔE9 proteins from cells expressing doxycycline-inducible FLAG-tagged HDAC7 cDNA isoforms or control (−cDNA). In, input; Un, unbound protein; IP, proteins eluted from beads following immunoprecipitation. Antibodies used are α-FLAG (for HDAC7 isoform), α-14-3-3, α-METTL14 (negative control), and α-LEF1. Band corresponding to anti-FLAG M2 light chain (from IP) is visible in IP lane blots with α-14-3-3 and is marked with an asterisk.
(G) Bar plot showing nanoL-C/MS-MS enrichment of 14-3-3 isoforms by HDAC7 protein iE9/ΔE9 isoform immunoprecipitation compared with bead-alone control.
See also Figure S3.

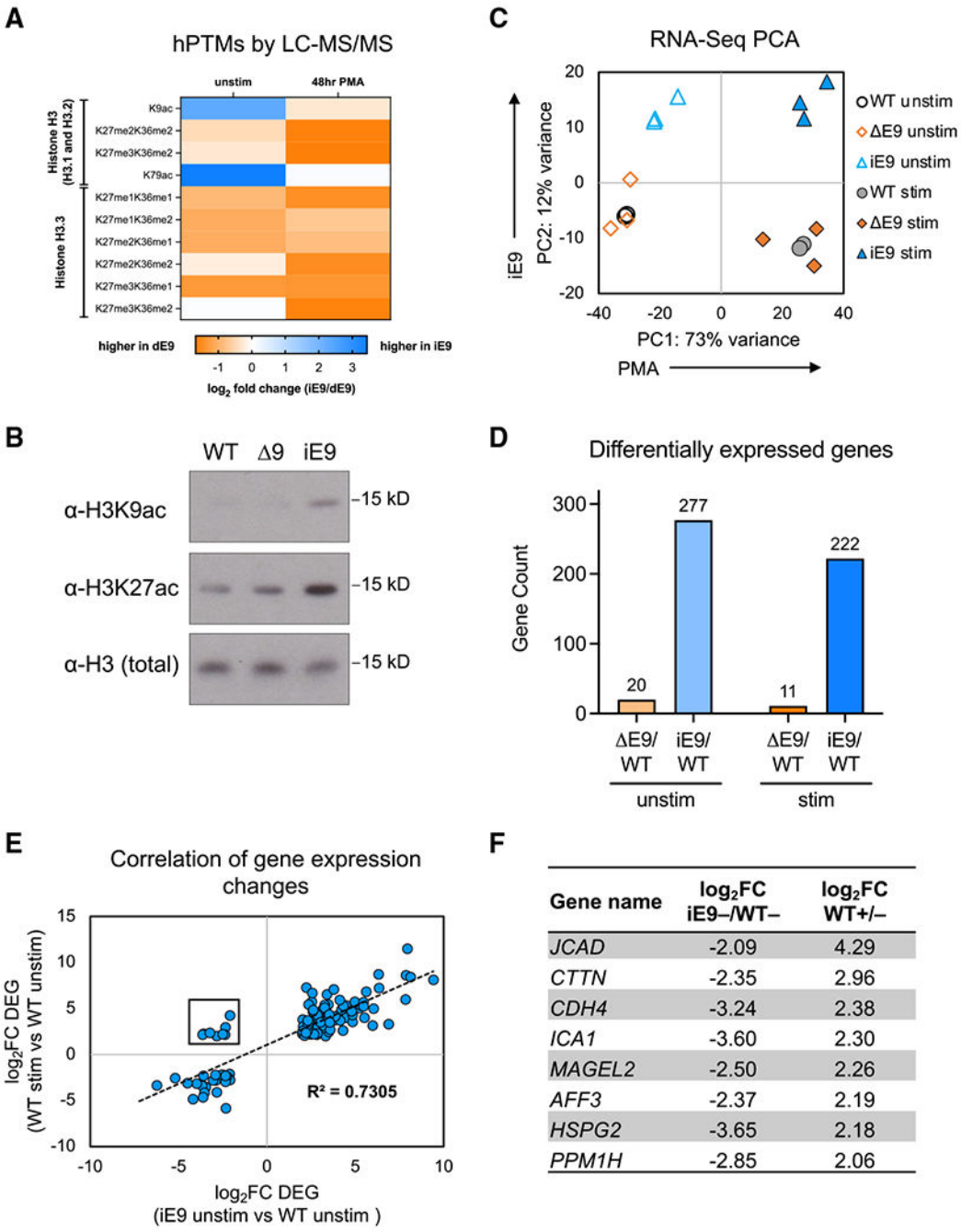

Gene name	log_2FC iE9–/WT–	log_2FC WT+/–
JCAD	-2.09	4.29
CTTN	-2.35	2.96
CDH4	-3.24	2.38
ICA1	-3.60	2.30
MAGEL2	-2.50	2.26
AFF3	-2.37	2.19
HSPG2	-3.65	2.18
PPM1H	-2.85	2.06

Figure 4. HDAC7 protein isoforms exhibit differences in histone post-translational modifications and gene expression

(A) Differences in histone post-translational modifications (hPTMs) in iE9 vs. ΔE9 CRISPR cell lines quantified by nano-LC-MS/MS. Full nano-LC-MS/MS analysis of hPTMs is shown in Figure S4B. Western blot analysis of total purified histones from WT (W) and CRISPR (i9 = iE9, Δ9 = ΔE9) cells with antibodies specific for the indicated modifications. (C) Principal-component analysis (PCA) plot of RNA-seq samples showing the main two differences (PCs 1 and 2, which account for 73% and 12% of the variance, respectively) between WT, iE9, and ΔE9 CRISPR cells in unstimulated and stimulated conditions

(individual replicates are plotted; symbols, border color, and filling color indicate the cell line ± 48 h PMA).

(D) Differentially expressed genes (DEGs) in WT vs. either CRISPR cell line. Filtering cutoffs were set to $\log_2$ fold change ≥|2| with an adjusted p value ≤ 0.05 and base mean ≥20. In total, there are 31 DEGs in ΔE9 cells and 409 DEGs in iE9 cells compared with WT cells.

(E) Correlation of expression in iE9 vs. WT (both unstimulated, x axis: $\log_2$ fold change ≥ |2|, adjusted p value [adj. p value] ≤ 0.05) compared with PMA-induced changes in WT cells (stimulated [stim] vs. unstimulated [unstim], y axis: $\log_2$ fold change ≥ |2|, adj. p value ≤ 0.05).

(F) A listing of the few genes that exhibit an opposite effect between iE9 and stimulated WT cells (boxed in E).

See also Figure S4.

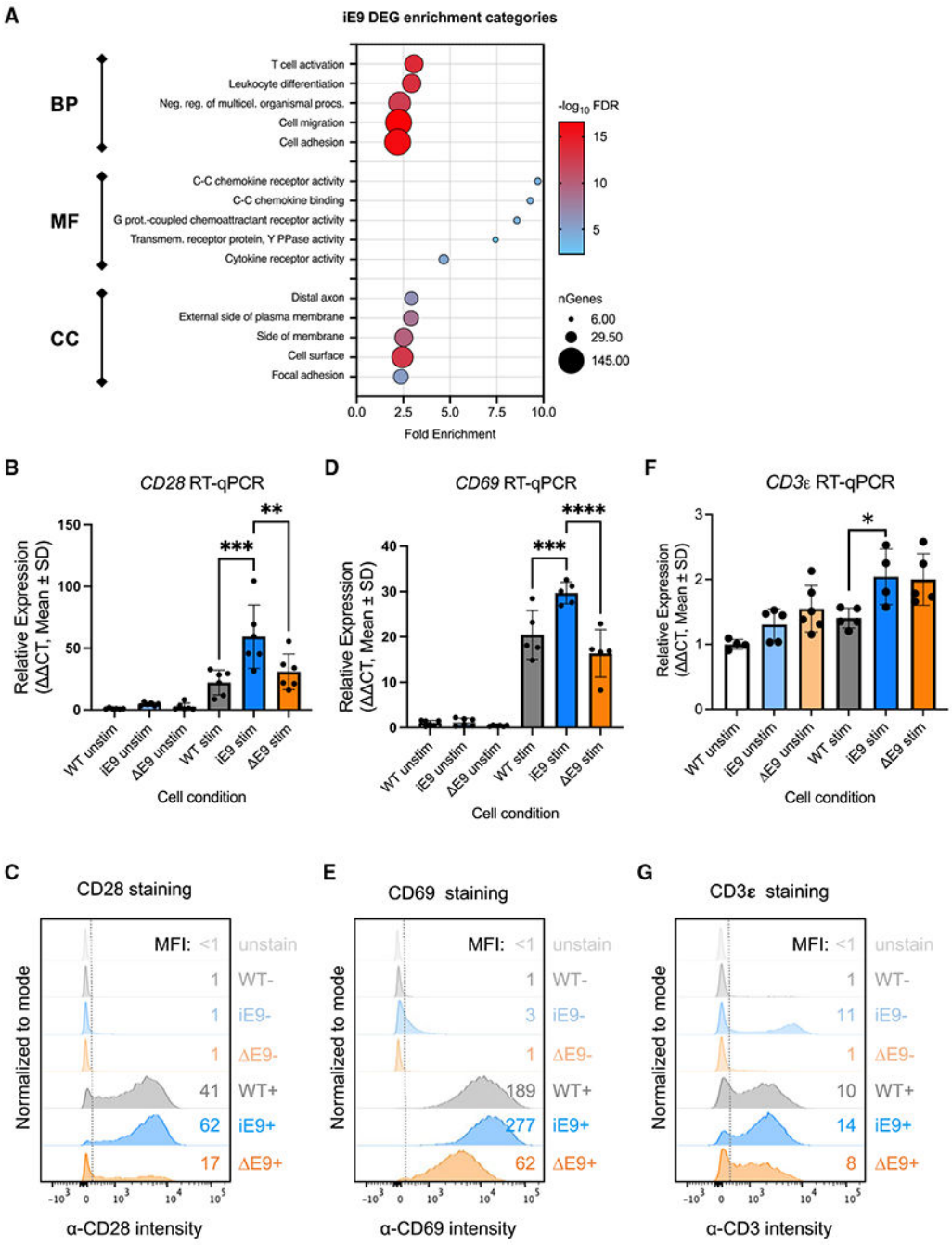

Figure 5. HDAC7 protein isoforms differentially regulate expression of T cell surface markers

(A) ShinyGO enrichment analysis of Gene Ontology (GO) biological process (BP), molecular function (MF), and cellular component (CC) categories enriched by the 409 iE9 DEGs (unstim+stim; Figure 4D). The y axis shows the top 5 enrichments divided by category and sorted from high to low fold enrichment.

(B) qRT-PCR experiment for *CD28* expression relative to *Actin* in WT vs. CRISPR cells (n = 6, ΔΔCT mean ± standard deviation, one-way ANOVA statistical test). (C) Representative flow cytometry data of CD28 cell surface expression, presented as offset modal histograms

across multiple cell populations (WT vs. CRISPR, unstim vs. stim, and an unstained negative control). The mean fluorescence intensity (MFI) of CD28+ is denoted on the right side of each histogram.

(D and E) Quantification of *CD69* as described in (B) and (C).

(F and G) Quantification of *CD3ε* as described in (B) and (C).

See also Figure S5.

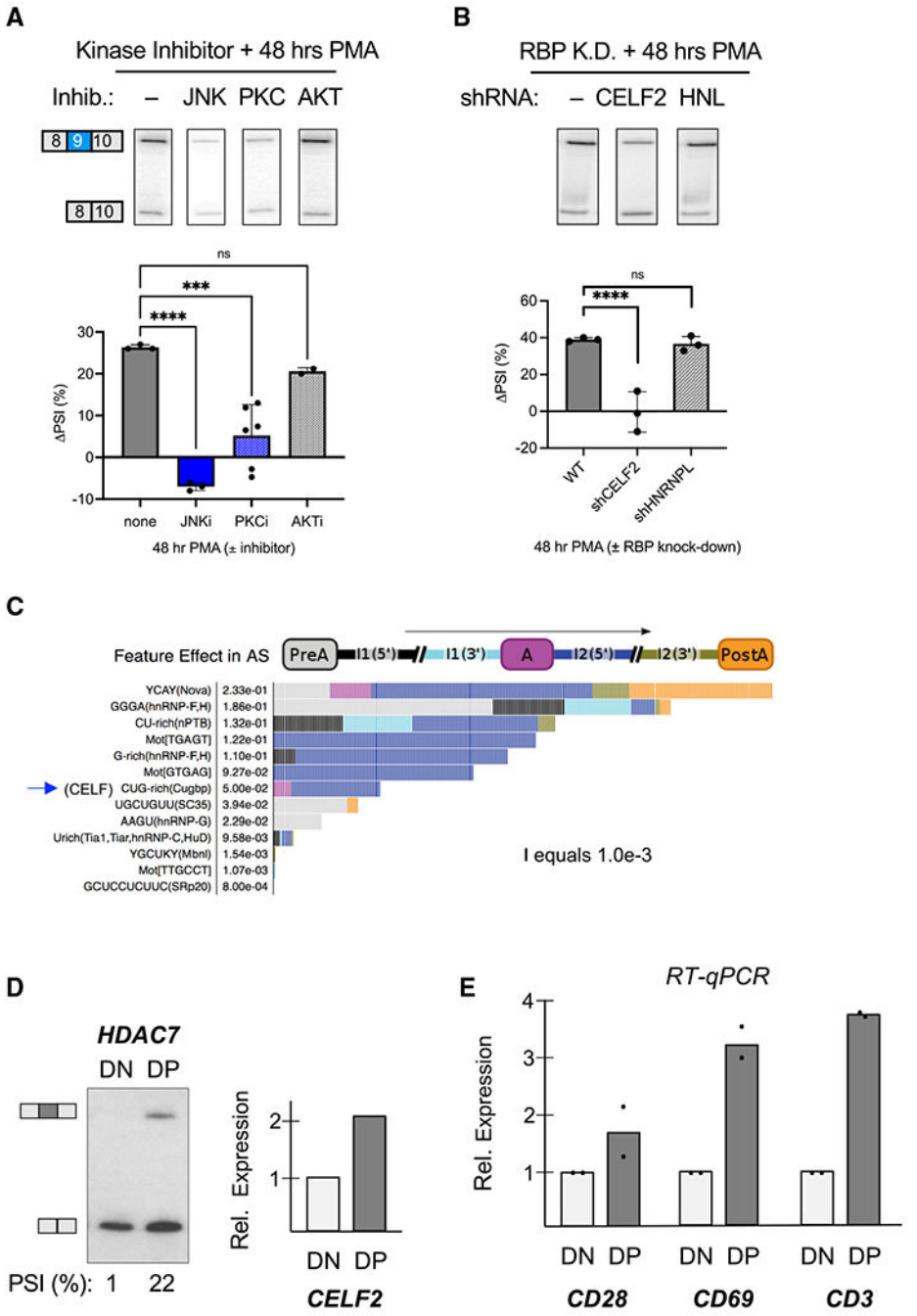

Figure 6. *HDAC7-E9* AS is regulated by CELF2 and JNK signaling

(A) Representative RT-PCR (top) and quantification (bottom) of HDAC7 splicing in stimulated JSL1 cells pre-incubated with small-molecule kinase inhibitors against the kinases shown (n = 2–6, one-way ANOVA statistical test). Products containing or lacking HDAC7 exon 9 are as indicated by the schematic to the left of the gels.

(B) Representative RT-PCR (top) quantification (bottom) of *HDAC7-E9* splicing in WT vs. RBP KD cells (n = 2–3, two-way ANOVA statistical test). All data are represented as the sample mean ± standard deviation.

(C) AVISPA analysis (Gazzara et al.[56]) of HDAC7 AS region indicating enrichment of motifs at indicated regions around alternative exon 9 (purple A) and surrounding genomic sequence. Arrow points to CELF2 binding motif.

(D) Left: RT-PCR of HDAC7 from fluorescence-activated cell-sorted (FACS) CFD4/CD8 double-negative (DN) and double-positive (DP) human thymocytes. Quantification of RT-PCR averaged from n = 2 replicates. Right: quantification of CELF2 as reported for these same thymocyte samples in Mallory et al.[32]

(E) qPCR quantification of CD3, CD28, and CD69 mRNA in thymocytes from (D). Dots indicate values from independent experiments (n = 2).

See also Figure S6.

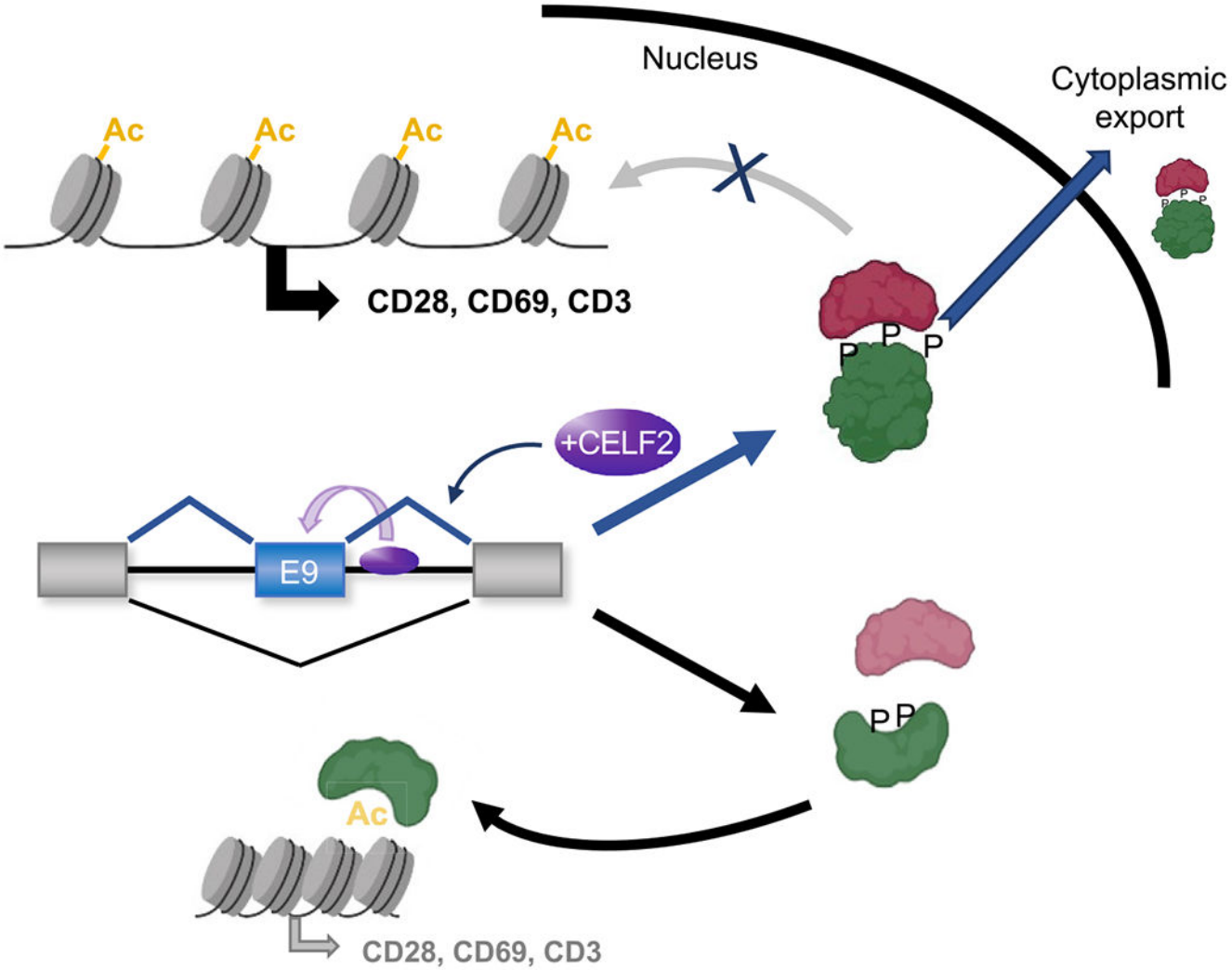

Figure 7. CELF2-driven AS of *HDAC7* alters target gene expression by controlling nuclear activity of HDAC7

Model based on data in this study and references therein regarding the regulation of *HDAC7-E9* splicing (blue box) by CELF2 (purple oval) and its functional consequence on the interaction of HDAC7 (green figure) with 14-3-3 (red figure), which promotes cytoplasmic localization, thus relocating HDAC7 away from chromatin (gray discs) and increasing histone acetylation (Ac) and corresponding gene expression of target genes such as CD3, CD28, and CD69.

See also Figure S7.

KEY RESOURCES TABLE

REAGENT or RESOURCE
Antibodies
HDAC7
Lamin-B1
PKM2
Flag
Pan-Histon H3
H3K9ac
H3K27ac
HnRNP L
Chemicals, peptides, and recombinant proteins
JNK inhibitor SP600125
PKC inhibitor Go6983
PKC inhibitor R0-31-8220
PKC inhibitor Sotrastaurin
AKT inhibitor MK2206
AKT inhibitor GDC-0068
RPMI 1640
Fetal bovine serum
MMLV
Bradford reagent
M2 affinity gel beads
Trypsin
Critical commercial assays
HiFi DNA Assembly kit
SYBR-based qPCR kit
Deposited data
Raw and analyzed RNA-Seq data
Raw and analyzed mass spectrometry data
Experimental models: Cell lines
Human: JSL1 cells (clonal Jurkat population)
Oligonucleotides
gBlock repair oligonucleotide: GCAGAACAATGCGCAGGACAGGGGGACAGAGATGGGGAGGAAGGATGGGTCCATCCCAAGCTTGGCTCTTAGCAGGGTGCAGGGACCCAGCCCCTTCCCTGAAC
HDAC7 E9 5′ splice site AMO: TGGGCACCCCAGCCACTCACCCTG
HDAC7 E4 5′ splice site AMO: CCGGGTTTGACTCTTACCTGCGC

REAGENT or RESOURCE
HDAC7 5′UTR: CCTCACATCCCCCCAGTCGCC
RT-PCR primers
RT-qPCR primers
sgRNAs
Recombinant DNA
pSpCas9(BB)-2A-GFP (PX458)
HDAC7 human ORF
Software and algorithms
CRISPick tool
STAR
ShinyGO
Sequest HT
DESeq2
rMATS